Characterization of a Dipole Flow System Using Point Velocity Probes

BY

Ian Reed Bowen
B.S., University of Kansas, 2008

Submitted to the graduate degree program Department of Geology
and the Graduate Faculty of the University of Kansas in partial fulfillment of the
requirements for the degree of
Master of Science.
2010

_____
Dr. J.F. Devlin, Chair

_____
Dr. Jennifer Roberts, Committee Member

_____
Dr. Don Steeples, Committee Member

Date Defended: November 22, 2010

The Thesis Committee for Ian Reed Bowen
certifies that this is the approved version of the following thesis:

Characterization of a Dipole Flow System Using Point Velocity Probes

_____
Chairperson Dr. J.F. Devlin

_____
Dr. Jennifer Roberts, Committee Member

_____
Dr. Don Steeples, Committee Member

Date approved:_____

Abstract

A direct groundwater velocity measurement tool, the Point Velocity Probe, was developed to measure velocities in the vertical and horizontal directions. The tool was designed and tested in a low-cost laboratory flow-through tank. Following testing, the tool was deployed in the field surrounding a dipole well used to conduct an aquifer tracer test. The velocity data showed some deviations from modeled behavior and was used to characterize the heterogeneity of the aquifer. The results from the flow and transport modeling suggest that the area very close to the well was extremely important to the behavior of tracers in the dipole flow system. Finally, a simple model was developed to optimize hydraulic conductivity using the velocity data with good results.

Acknowledgements

I would first like to thank my advisor, Dr. Rick Devlin, for the mentorship, review efforts, and all the other work over many years and several projects. However, it is your friendship that I appreciate most, so thank you. I must also thank Dr. Neil Thompson, University of Waterloo, for providing me the opportunity to perform this study. Ashley Mathai and Kat McLean, also at the University of Waterloo, deserve special recognition for spending countless hours in the field collecting data. Thank you to Peter Schillig for all the help, training, time and life saving advice. If it weren't for you, I wouldn't know how good I had it. One of these days we might finally build that deck. Thank you to Alek McElroy for your help in laboratory testing of the mini-PVPs.

Many other people at the University of Kansas provided assistance on this project. I would especially like to thank Dr. Jennifer Roberts for reviewing, teaching, and mentorship. I'd also like to thank Dr. Don Steeples and Dr. Leigh Stearns for their help reviewing this manuscript.

Several other people at the University of Waterloo deserve recognition. Bob Ingleton, Paul Johnson, Steve Chai, and Terry Ridgway helped assemble, install, and troubleshoot equipment and made my life much easier while in Ontario.

Finally, I must thank my wife, my friends, and my family for always being there when I needed support.

This work was funded by Dr. Neil Thompson at the University of Waterloo.

Table of Contents

List of Tables

List of Figures

.

Chapter 1: Introduction

1.1 The Importance of Groundwater Velocity in Aquifer Characterization

Accurate site characterization has always been a necessary step in contaminant remediation. As technology has advanced, more detailed site-specific data have become necessary. The rise of passive *in situ* remediation strategies has placed an emphasis on understanding groundwater velocity patterns at sites, and the role velocity plays in contaminant transport (Gavaskar, 1999; Labaky *et al.*, 2007). Detailed groundwater velocity data can be obtained with the Point Velocity Probe (PVP), which is capable of directly measuring groundwater velocity at the centimeter scale without a well (Labaky *et al.*, 2007).

This investigation has centered on furthering the development of the Point Velocity Probe in the laboratory and field. First, a laboratory testing apparatus, the Nested Storage Tank, was designed and constructed to provide an inexpensive bench top device for testing the PVP (Chapter 2). The Nested Storage Tank was used to laboratory test a new PVP design capable of measuring horizontal and vertical flow (Chapter 3). Following testing, the PVP was deployed around a pumping well to characterize a dipole flow system (Chapter 4), and the velocity data measured were used to optimize hydraulic conductivity information in a simple flow model (Chapter 5).

1.2 The Scale Dependence of Groundwater Velocity Measurements

Characterizing groundwater velocity is very important for determining contaminant transport pathways and residence times in remediation systems.

The need for small-scale estimations is particularly important when *in situ* remediation schemes are employed because contaminant mass distribution within a plume is highly variable spatially and temporally (Morkin *et al.*, 2000; Guilbeault *et al.*, 2005). Guilbeault *et al.* (2005) showed a 15 cm sampling interval was necessary to characterize important centimeter scale features in several plumes. While these variations are related to heterogeneity, the heterogeneity is equally related to hydraulic conductivity, *K*, and therefore groundwater velocity. Even if *K* can be measured and the distribution defined at this scale, other hydraulic parameters necessary to calculate velocity – such as hydraulic gradient – are unlikely to be fully measurable at the same scale. This has negative implications for remediation design (Gierczak *et al*. 2006).

As alluded to above, conventional methods for determining velocity are largely based on indirect estimates using Darcy's Law (Fetter, 2001). The method involves a calculation requiring knowledge of the hydraulic gradient, the hydraulic conductivity and porosity for a site (or specific location). These parameters may be difficult to estimate accurately and precisely for small areas such as those associated with contaminant transport and remediation treatment zones.

The indirect technique is usually considered limited by the need for accurate aquifer K estimates (Ballard, 1996; Butler, 1997). Representative K values are difficult to obtain because this property can vary by orders of magnitude over short distances, and values may also vary with the type of measurement method used (Sudicky, 1986; Butler, 2005). *K* is typically

estimated with pumping tests, slug tests, or laboratory core analysis. In a pumping test, a large volume of aquifer is sampled and provides a relatively large scale average estimate of the *K*. However, aquifer tests do not provide the detailed information about the variations in *K* at a scale relevant to many contaminant transport investigations (Butler, 2005). Slug tests estimate *K* close to a well, and high-resolution slug tests are capable of providing *K* profiles at small intervals (approximately 10 centimeters) (Labaky, 2009). Aquifer material obtained from cores can also be used to provide very detailed *K* distributions (usually centimeter-scale vertical distributions) (Sudicky, 1986). While the sampling intervals of slug tests and core analysis are small enough to provide information relevant to treatment zones, they require an extensive sampling network to properly characterize heterogeneity, and the *K* distributions are insufficient on their own to permit a velocity field to be defined.

Once *K* is well defined, the calculation of velocities may be limited by the quality of hydraulic gradient estimates. The error associated with the measurement of hydraulic heads may limit the precision with which an hydraulic gradient can be determined. For example, Devlin and McElwee (2007) reported work involving a highly conductive aquifer in which the gradient could not be determined reliably over a ~500 m^2 region.

The limitations of indirect velocity determination can be overcome by direct velocity measurements. While the Point Velocity Probe was selected for the work described in this thesis, a number of other technologies exist that might be useful in other situations. Examples that have received notable attention in the

past include the colloidal borescope, borehole dilution, the VECTOR® Groundwater Flowsensor, the Geoflo® meter, and natural and forced gradient tracer tests (Ballard, 1996; Kearl 1997; Labaky *et al.*, 2009).

The technologies listed above operate at a variety of scales. The PVP is discussed in detail in Chapter 3 and operates at the centimeter scale. The colloidal borescope velocity estimate could be averaged over a volume as small as 1 mm^3 as estimated by Ballard (1996), however if many measurements were averaged, the effective scale could be larger (Kearl, 1997; Labaky *et al.*, 2009). Borehole dilution has been used to determine velocity profiles in wells at small intervals (tens of centimeters), but is limited to horizontal velocities (Pitrak *et al.,* 2007). The scale of the velocity estimates generated by the VECTOR® Groundwater Flowsensor and the Geoflo® meter are limited by the sizes of the instruments, or the well screens in which they operate. In the case of VECTOR® Groundwater Flowsensor, the tool is 75 cm long. Ballard (1996) suggests that the VECTOR® Groundwater Flowsensor provides a velocity estimate averaged over a nearly 1 m^3 volume which is contrasted with a 1000 cm^3 volume for the Geoflo® meter.

Finally, tracer tests involve the injection of a tracer into the subsurface and monitoring its transport due to ambient or forced groundwater flow. This type of test yields velocities that are averaged over the distance between the measurement points (often 10s of meters)

1.3 The Dipole Recirculation Well and Reactive Tracer Test

The field test of the new PVP designed in this work involved mapping the velocity field around a dipole recirculation well. A dipole well is one that both injects water to the subsurface and withdraws it, so flow recirculates through the aquifer around the standpipe. To create the dipole well used in this work, packers were used to isolate two sections of a continuous well screen so that water could be injected through one and extracted from the other. This resulted in a recirculating system with both horizontal and vertical components to flow in the surrounding aquifer. Such flow systems are difficult to characterize experimentally because the flow pattern is both complex and concentrated in a relatively small volume. Unless flow rates are substantial, conventional methods of tracking groundwater movement, i.e., using hydraulic head measurements, are likely to be inadequate in a system like this. Therefore, the dipole flow system provided an ideal location to test PVPs.

Practical uses of the dipole packer apparatus inserted into a well include the acquisition of *K* profiles with depth, and the assessment of microbial activity in an aquifer through the use of reactive tracers (Reiha, 2006; Roos, 2009). With the latter use in mind, a flow model was created to simulate and match conservative and reactive tracer breakthrough curves from a field test termed the Dipole Flow and Reactive Tracer Test, DFRTT. In preliminary work, the results of DFRTTs at the CFB Borden site, in Ontario, Canada, suggested that a homogeneous aquifer model was insufficient to replicate the experimental breakthrough curves. The DFRTT breakthrough data showed earlier arrival

times than expected from the model, as well as discrepancies in the tail of the breakthrough curves (Roos, 2009).

Determining the area of influence of a dipole well is a common goal of studies involving these technologies. The results of previous work are mixed, but most suggest the area of influence is difficult to characterize and usually smaller than predicted using groundwater models (U.S. EPA, 1999; U.S. EPA, 2000; Johnson and Simon, 2007). Factors contributing to this include anisotropy and heterogeneity of the formation that are not properly taken into account in the models. However, limitations in the numerical models themselves may also contribute to these disagreements (EPA, 1999; Johnson and Simon, 2007).

At least one previous study has reported direct measurements of groundwater velocity surrounding a dipole well (Johnson and Simon, 2007). In that case, the velocities were measured with the VECTOR Groundwater Flowsensor, which operates by relating temperature distributions on a 0.75 m to 1 m long heated, cylindrical probe to groundwater velocity. The Vector Flowsensor was not able to reliably measure vertical velocities and therefore much of the flow system in that work could not be adequately defined (Su *et al.*, 2006; Johnson and Simon, 2007). The authors remarked on the their disappointment in the quality of the direct velocity measurements, and the inability of the flow system mapping to establish a hydraulic connection between the extraction and injection portions of the capture zone. At least some of the problems associated with this attempted mapping exercise may have been due to the scale of the velocity measurements.

Most of the methods available for making groundwater velocity estimations provide an estimate of velocity averaged over a scale too large to be helpful in characterizing flow around the DFRTT. The PVP is a promising tool that provides measurements at the centimeter scale using a low-cost, easy to install probe that is able to return velocity estimates in a reasonable time frame (within 1 day) (Labaky *et al.*, 2007; Devlin *et al.*, 2009). This tool is one of the few capable of measuring vertical and horizontal velocities at the centimeter scale allowing the characterization of a dipole induced flow system in unprecedented detail.

1.4 Thesis Objectives

The objectives of this thesis are to:

1. Design, construct, and test a simple, inexpensive, and leak resistant apparatus suitable for creating a controlled flow system in a porous medium at the benchtop scale. The apparatus is to be used in achieving objective 2, below.
2. Design, construct, laboratory test, and field-test a prototype PVP capable of measuring horizontal and vertical flow.
3. Design, construct, and field-test a device capable of measuring groundwater velocity in the well skin of an operating dipole well.
4. Characterize the flow system around a dipole well to assist in the simulation of tracer movement in the aquifer during a DFRTT with a numerical model.

Chapter 2.

A Simple, Low-Cost, Leak-Resistant Flow Through Tank

2.1 Introduction

Laboratory investigations involving flow and transport are essential for understanding many groundwater systems because they provide a controlled environment in which to study flow and transport (Silliman, 1998; Danquigny *et al*., 2004). The most important benefits to of these tests are that the boundary conditions and properties of the porous medium can be highly constrained and simplified, or at least characterized in great detail (Silliman, 1998). Laboratory models allow selected processes to be isolated and studied under controlled, repeatable conditions and are less expensive than field experiments (Silliman, 1998; Danquigny *et al*., 2004; Close *et al*., 2008). The purpose of this work was to develop a low-cost benchtop tank system to study flow and transport, hereafter referred to as the Nested Storage Tank (NeST).

Many laboratory-scale aquifer models have been developed since Darcy's (1856) column experiments. Flow and transport experiments are still commonly conducted in one-dimensional columns (Sternberg *et al*., 1996; Watson *et al*., 2002; Bi *et al*., 2009), but for some investigations one-dimensional flow is insufficient to meet the experimental needs. For example, two-dimensional physical models, often used to visualize flow systems, have been used to study the effect of heterogeneity on transport (Silliman *et al*., 1998; Barth *et al*., 2001). There have also been physical models developed to study radial flow around

wells (Simpson *et al*., 2003). Finally, A variety of tanks to study three-dimensional flow have been developed. Most are of benchtop scale (Danquigny *et al*., 2004), such as the one presented in this article, but there are also several large simulated aquifers reported in the literature (Close *et al*., 2008; Lee *et al*., 2008; Kobus *et al.* 1996).

A drawback to the use of benchtop tanks is that they are not commercially available, except for some small teaching kits. Custom built tanks are moderately costly to build, and are often subject to leakage. In some tank designs, uniform flow is not achieved (Patterson *et al.*, 2010). The NeST, which can be easily constructed for about $50 from readily available parts, using common tools, was demonstrated to create a highly uniform flow system, and was used to compare and contrast several methods of estimating average linear velocities in porous media.

2.2 Methods

2.2.1 NeST Design

The NeST uses a three-compartment system consisting of two open water reservoirs and an intermediate porous medium container. In the experiments performed for this project, water was pumped at a constant flow rate between the open-water reservoirs, creating an hydraulic gradient – and consequently flow – through the porous medium. The first compartment consisted of a tall plastic storage container in which high water levels could be maintained. The second compartment, later packed with a porous medium, was connected to the first with

9 short, plastic irrigation fittings distributed evenly over the entire upgradient side of the container. The first two compartments were seated inside the third, which received flow from the porous medium compartment through about 400 small holes drilled into the downgradient end of that container (Figures 1 and 2). Sand was contained within the second compartment by lining the irrigation fittings and the effluent end of the compartment with Nitex mesh. Because all the compartments were made of single pieces of molded plastic, the potential for leakage was very low.

2.2.2 NeST Construction and Packing

The NeST design makes use of inexpensive, readily available plastic storage bins, irrigation pipe-fittings, and screen (Table 1), and construction of the tank requires little more than a drill and handsaw. The upgradient compartment (1 in Figure 3) was connected to the porous medium compartment (2 in Figure 3) by cutting away the rim of the latter to allow continuous contact between the compartment sides. Holes were then drilled for the irrigation fittings (Figure 2), which were fastened in place with a garden hose washer and nut so that the two compartments were held tightly together. A small amount of silicone caulking between the fittings and the holes was sometimes necessary to assure a good seal. Nytex mesh was placed inside the nuts to prevent sand from entering the first compartment through the fittings.

Next, the downstream end of the sand compartment was perforated with about 400 1/16” holes, using an electric drill. The first and second

compartments, now held together with the fittings, were placed into the third. Nytex screening was then draped over the downgradient side of compartment 2, covering the holes and preventing the porous medium from escaping compartment 2 into compartment 3.

Finally, compartment 2 was wet packed with a porous medium – sand in the case of the experiments reported in this work. Wooden braces, held in place with clamps, were used to prevent the tank from deforming due to the pressure of the saturated porous medium (Figure 3). After packing the tank, a peristaltic pump moved water out of compartment 3 and into compartment 1. This created an hydraulic gradient across the porous medium in compartment 2, and flow ensued.

2.2.3 Tracer Tests

Three types of the tracer tests were performed to estimate the average linear velocity inside the NeST, and to permit an assessment of the degree of uniformity of the flow system generated. The measured velocities were compared to velocity estimates derived from equation 1: where Q is the flow rate (Volume/Time), n (dimensionless) is the porous medium (sand) porosity, and A (Length^2) is the cross sectional area of compartment 2.

$$v = \frac{Q}{An} \qquad (1)$$

In the first tracer test, the water level in compartment 2 was raised to fully saturate the sand medium without creating any ponding on the surface. A dye

(blue food coloring) was applied to the sand surface and its transport was tracked visually (Figure 4).

The second test consisted of a constant-source salt tracer experiment. A concentrated NaCl solution was added to compartment 1 to instantaneously increase the salt concentration entering compartment 2 from <50 mg/L to about 1000 mg/L NaCl, increasing the conductance of the water accordingly. Conductivity detectors were installed in the NeST during packing and used to monitor arrival times of the tracer. Velocities were estimated by fitting the breakthrough curves with a model based on the Ogata-Banks (1961) solution to the advection dispersion equation (Figure 5a).

The third test for velocity estimation was performed using a point velocity probe (PVP), as described by Labaky *et al.* (2007). The PVP determines velocity by monitoring tracer transport around a cylindrical probe (see Chapter 3 for details). Briefly, this test also produced breakthrough curves, which were modeled to determine the average linear velocity of water in compartment 2 (Figure 5b).

2.2.4 Porosity Estimation

It is apparent from equation 1 that velocity estimation depends upon a reasonable knowledge of the porous medium porosity. Two methods for measuring porosity were used in this work. First, an approximately 15 cm core of sediment was collected from the NeST after the tracer tests were complete. The core was weighed wet and later dry, and the porosity estimated gravimetrically.

Since core collection can deform the sample, biasing porosity measurements, a second method was also used. The sand was wet packed into a 600 mL beaker in a fashion similar to the packing procedure in the NeST. Again the porosity was determined gravimetrically.

2.3 Results and Discussion

The software suite, Visual MODFLOW PRO, was used to assess the distribution of non-uniform flow near the inlet, due to the presence of 9 discrete entry points for flow. Constant-head boundary locations were used to represent the irrigation fittings, as well as the open water column at the downgradient end of the sand compartment (Figure 6). No-flow boundaries were used to surround the rest of the model domain. The simulations indicated that irregularities associated with the irrigation fittings on the upgradient boundary were limited to no more than 10 cm from the boundary. Boundary effects were minimal in the center of the box where the PVPs were located.

Experiments were performed at various flow rates to evaluate the comparability of the various tracer test methods (Figure 7, Table 2). In general, the estimated velocities agreed quite well, with nearly all measurements within ±25% of one another. This is encouraging because the tests operate on different principles with slightly different scales of measurement.

The velocity obtained from equation 1 was based on relatively certain knowledge of the flow rate and cross sectional area of the tank. The porosity of

the sand was estimated to be 0.52 ± 0.13, which was primarily responsible for the uncertainty in velocity estimated this way.

The visual tracer test and constant source tracer test were conducted in similar fashions. They both yielded an average velocity between the source and a monitoring location and, as expected, agreed well. It is possible that small biases were introduced in the visual tracer test due to variability at the sand surface, since it represents a boundary.

The PVP operates at the centimeter scale, and the velocity was therefore not averaged over a distance as it was in the other tests. Velocities measured at single points are expected to exhibit more variability than spatially averaged velocities, like those estimated in the visual and constant source tests, even though the point measurement are collected with high precision. Nevertheless, the PVP velocities agreed well with those estimated by the other methods.

The uniformity of flow in compartment 2 was indicated two ways. First, the progress of the visual tracer was remarkably even across the tank, showing that no dominant preferred flow path existed, at least near the surface. Second, the reasonable agreement in velocity estimates from the various methods – which were based on flow in different parts of the tank – suggests that flow in the NeST apparatus was quite uniform and well behaved. On this basis, the NeST is judged to be capable of creating and sustaining a uniform flow field through the porous medium compartment.

Although hydraulic gradients were not measured in this work, it was noted in several experiments (data not shown) that the top of the saturated zone in the

sand was visible through the translucent sides of the compartments. Therefore, the possibility exists for experiments to be performed, in homogeneous material, utilizing direct gradient measurements in addition to the methods described above.

2.4 Conclusions

The results of this work demonstrate that the NeST system is an inexpensive, functional apparatus for bench-scale flow and transport experiments. Three independent tracer tests yielded very similar estimates of the average linear velocity in a sandy medium, indicating the NeST could produce a nearly uniform flow field in the tank, and that the system constitutes a reliable benchtop apparatus for experimental work. The NeST is simple to build, inexpensive, and not prone to leaks. The system is therefore suitable for teaching applications as well as research purposes.

Table 2.1: Parts required in the construction of a NeST

Part Name	Quantity
Irrigation Fittings	9
Large Storage Container	1
Medium Storage Container	1
Tall Container	1
Hose Washers	18
Nytex Mesh	6 ft^2

Table 2.2: Summary of the velocity estimates acquired using the NeST. The uncertainty represents one standard deviation for each flow rate and type of measurement.

Test Type	Discharge (mL/min)	Measured Velocity (cm/day)	Expected Velocity from Equation 1 (cm/day)
PVP	3.5 ± 1.2	14 ± 4	16 ± 2
PVP	2.3 ± 1.2	9 ± 4	4 ± 1
PVP	4 ± 1.2	16 ± 4	13 ± 2
PVP	4.1 ± 1.2	16 ± 4	14 ± 2
PVP	3.3 ± 1.2	13 ± 4	12 ± 2
PVP	11 ± .5	44 ± 2	37 ± 6
PVP	12 ± .5	48 ± 2	42 ± 6
PVP	10.6 ± .5	43 ± 2	38 ± 6
PVP	10.4 ± .5	42 ± 2	40 ± 6
PVP	17 ± .5	68 ± 6	59 ± 9
PVP	18 ± .5	72 ± 6	73 ± 11
PVP	18.2 ± .5	73 ± 6	71 ± 11
PVP	18 ± .5	72 ± 6	69 ± 11
PVP	62 ± .5	257 ± 23	249 ± 57
PVP	62 ± .5	245 ± 23	249 ± 57
PVP	62 ± .5	294 ± 23	249 ± 57
PVP	62 ± .5	294 ± 23	249 ± 57
PVP	70 ± .5	281 ± 23	292 ± 57
Continuous Salt Tracer	3 ± 1.2	16 ± .3	12 ± 2
Continuous Salt Tracer	3 ± 1.2	17 ± .3	12 ± 2
Continuous Salt Tracer	3 ± 1.2	17 ± .3	12 ± 2
Continuous Salt Tracer	3 ± 1.2	17 ± .3	12 ± 2
Continuous Salt Tracer	11 ± .5	35 ± 6	38 ± 6
Continuous Salt Tracer	11 ± .5	25 ± 6	38 ± 6
Continuous Salt Tracer	11 ± .5	37 ± 6	38 ± 6
Continuous Salt Tracer	11 ± .5	40 ± 6	38 ± 6
Continuous Salt Tracer	11 ± .5	41 ± 6	38 ± 6
Continuous Salt Tracer	17 ± .5	41 ± 5	62 ± 6
Continuous Salt Tracer	17 ± .5	50 ± 5	62 ± 6
Continuous Salt Tracer	17 ± .5	48 ± 5	62 ± 6
Continuous Salt Tracer	67 ± .5	312 ± 7	233 ± 54
Continuous Salt Tracer	67 ± .5	312 ± 7	233 ± 54
Continuous Salt Tracer	67 ± .5	300 ± 7	233 ± 54
Visual Tracer	3 ± 1.2	14 ± 3	12 ± 2
Visual Tracer	3 ± 1.2	9 ± 3	12 ± 2
Visual Tracer	3 ± 1.2	7 ± 3	12 ± 2
Visual Tracer	3 ± 1.2	7 ± 3	12 ± 2
Visual Tracer	3 ± 1.2	6 ± 3	12 ± 2
Visual Tracer	3 ± 1.2	6 ± 3	12 ± 2
Visual Tracer	11 ± .5	47 ± 7	38 ± 6
Visual Tracer	11 ± .5	39 ± 7	38 ± 6
Visual Tracer	11 ± .5	34 ± 7	38 ± 6
Visual Tracer	17 ± .5	38 ± 3	62 ± 6
Visual Tracer	17 ± .5	36 ± 3	62 ± 6
Visual Tracer	17 ± .5	35 ± 3	62 ± 6
Visual Tracer	17 ± .5	40 ± 3	62 ± 6
Visual Tracer	17 ± .5	33 ± 3	62 ± 6
Visual Tracer	67 ± .5	289 ± 20	233 ± 54
Visual Tracer	67 ± .5	262 ± 20	233 ± 54
Visual Tracer	67 ± .5	255 ± 20	233 ± 54
Visual Tracer	67 ± .5	240 ± 20	233 ± 54

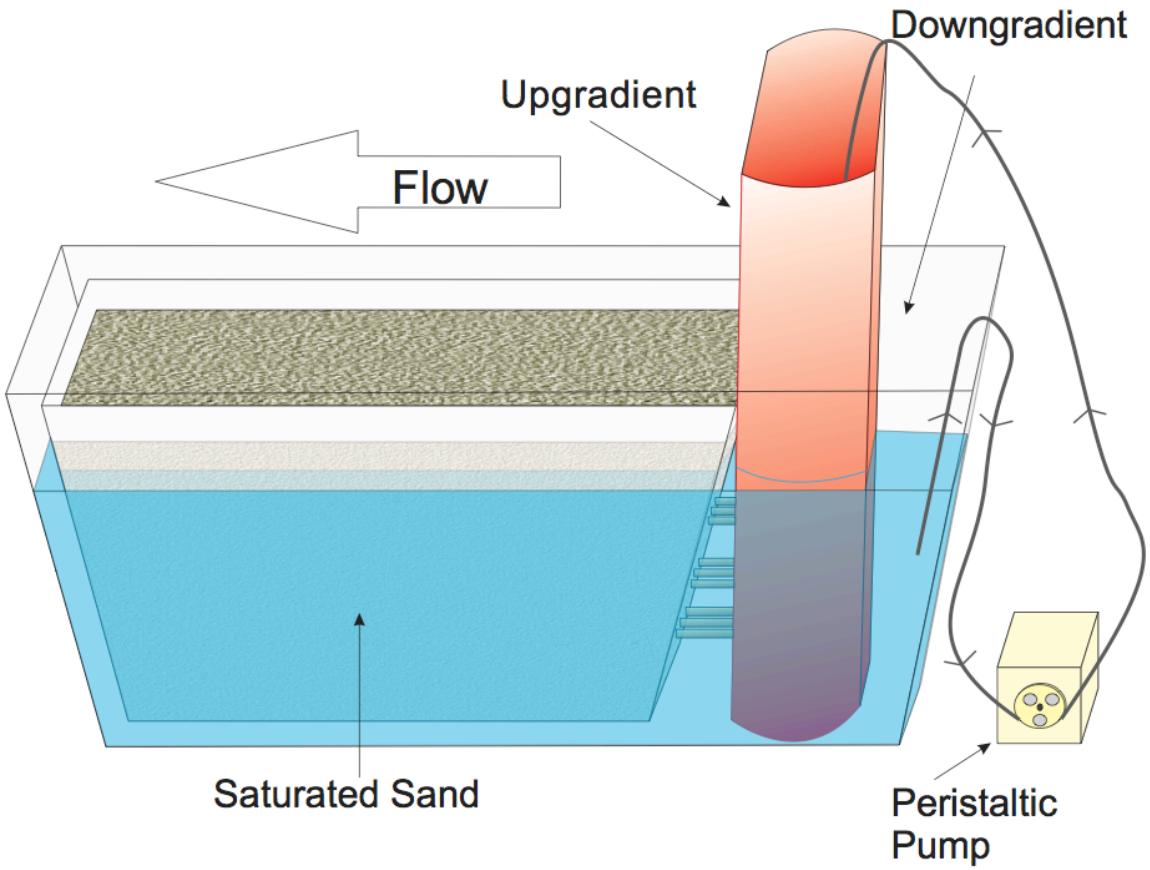

Figure 2.1: Schematic of the NeST system shows how the upgradient, porous media, and downgradient compartments are connected.

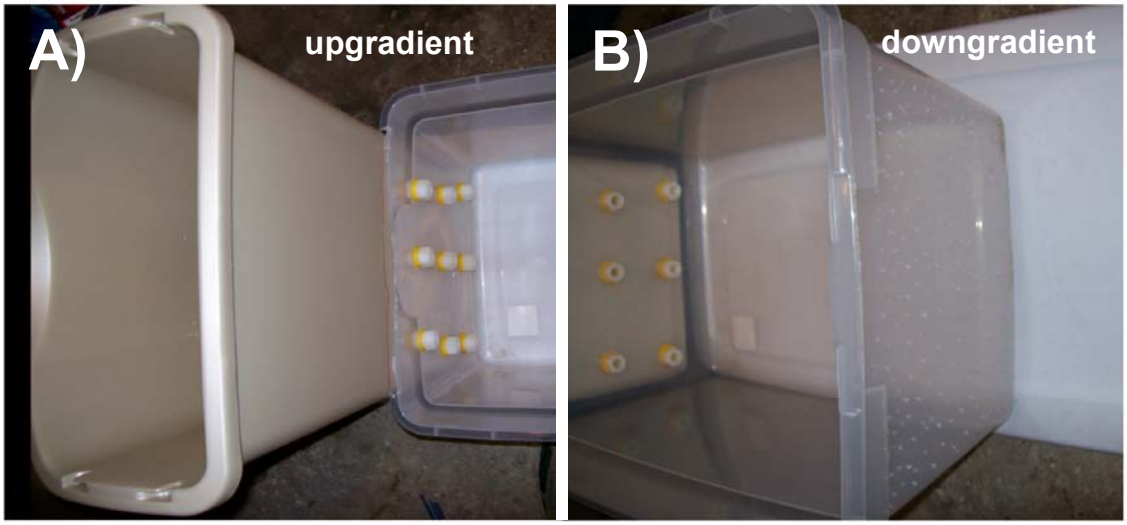

Figure 2.2: Construction of the NeST system. The first and second (porous medium) compartments are connected with irrigation fittings, and the second and third compartments (third not shown) are connected via drilled holes on the downgradient end of the second compartment.

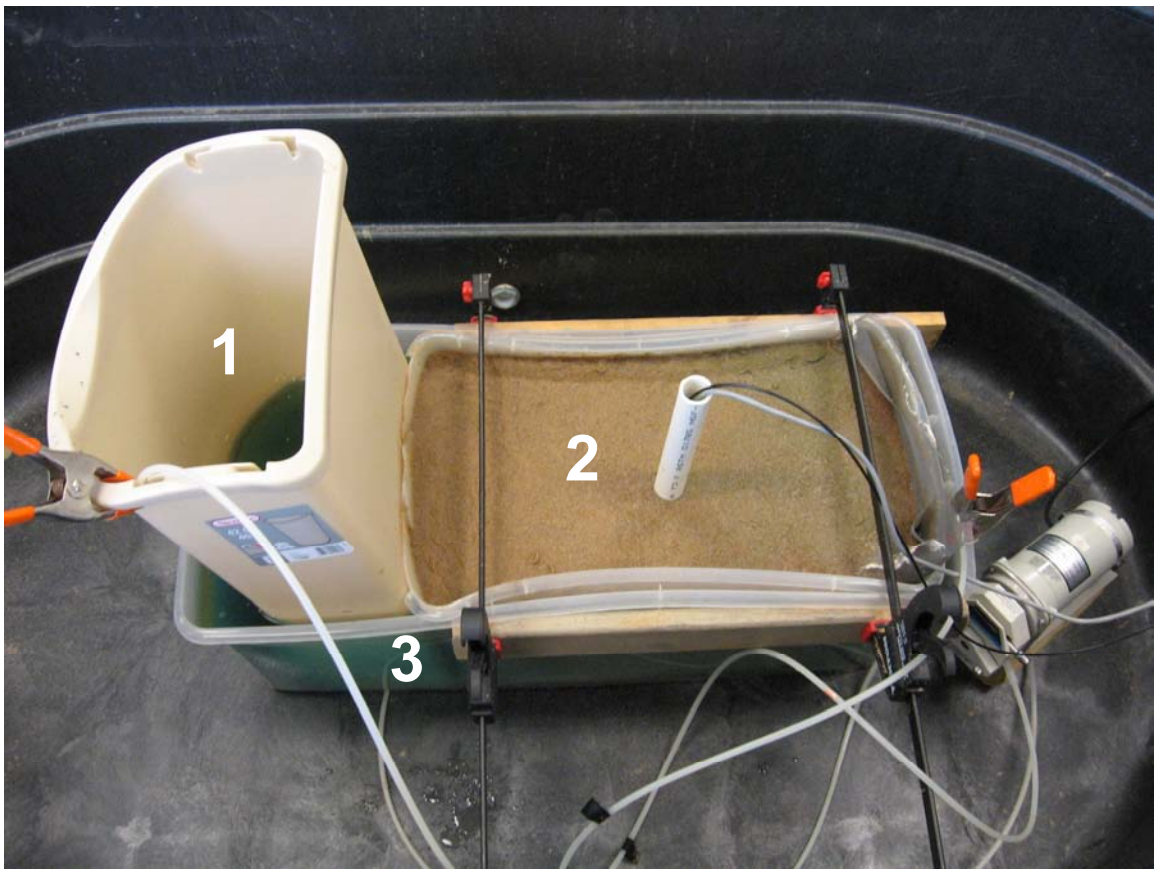

Figure 2.3: The completed NeST with a point velocity probe deployed. Compartments are labeled in a fashion consistent with the text.

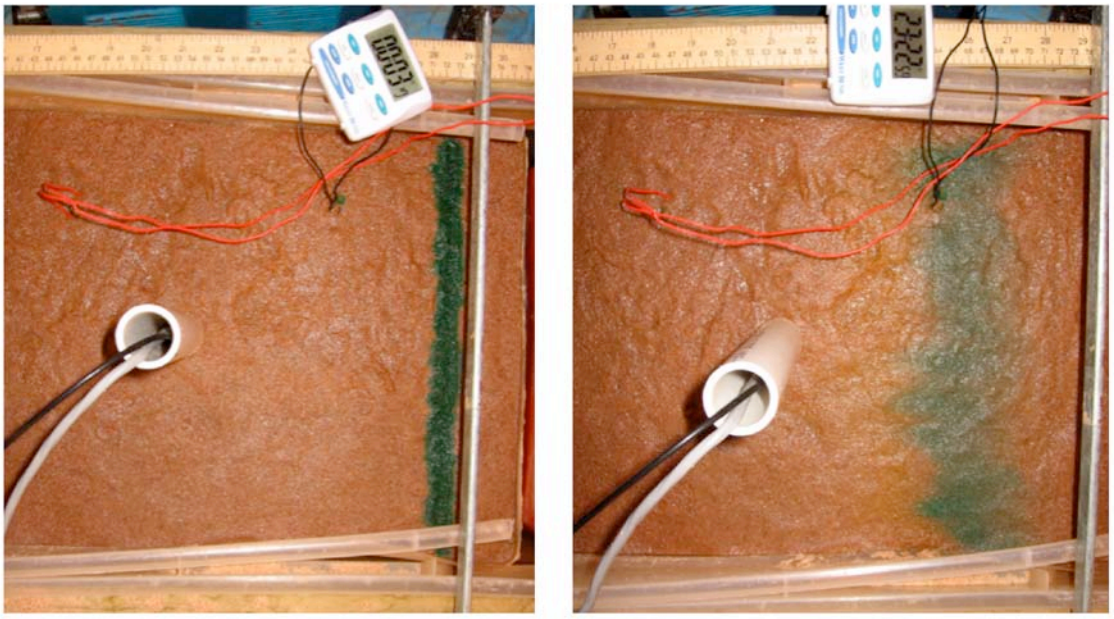

Figure 2.4: Tracer test conducted at 3 mL/min pumping rate resulting in a velocity of 17 cm/day. This result is near the 12 cm/day calculated using Equation 1. Furthermore, the tracer test shows that flow is quite uniform laterally with a 3 mL/min pumping rate.

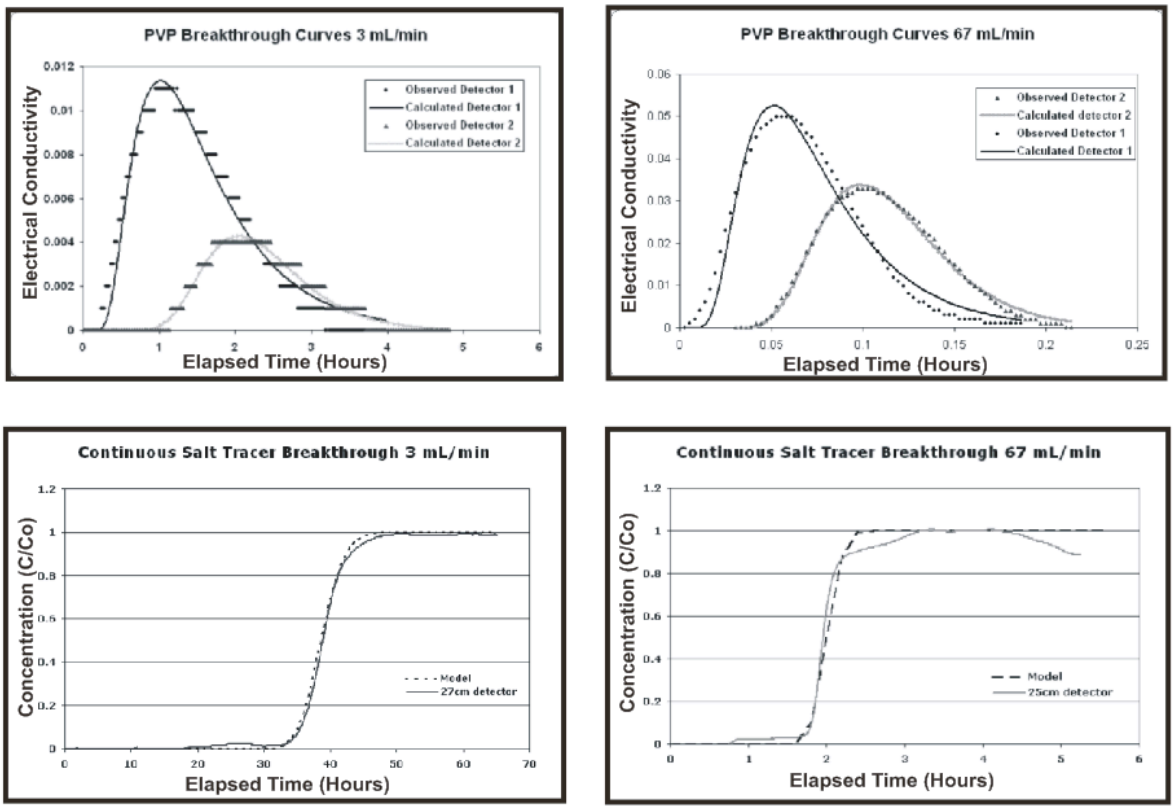

Figure 2.5: Example breakthrough curve data from the continuous salt tracer tests and PVP tests at a pump rate of approximately 3 mL/minute and 67 mL/minute. As seen here, the models were in good agreement with the measured data and the velocity estimates agreed well with expected values and other velocity estimates.

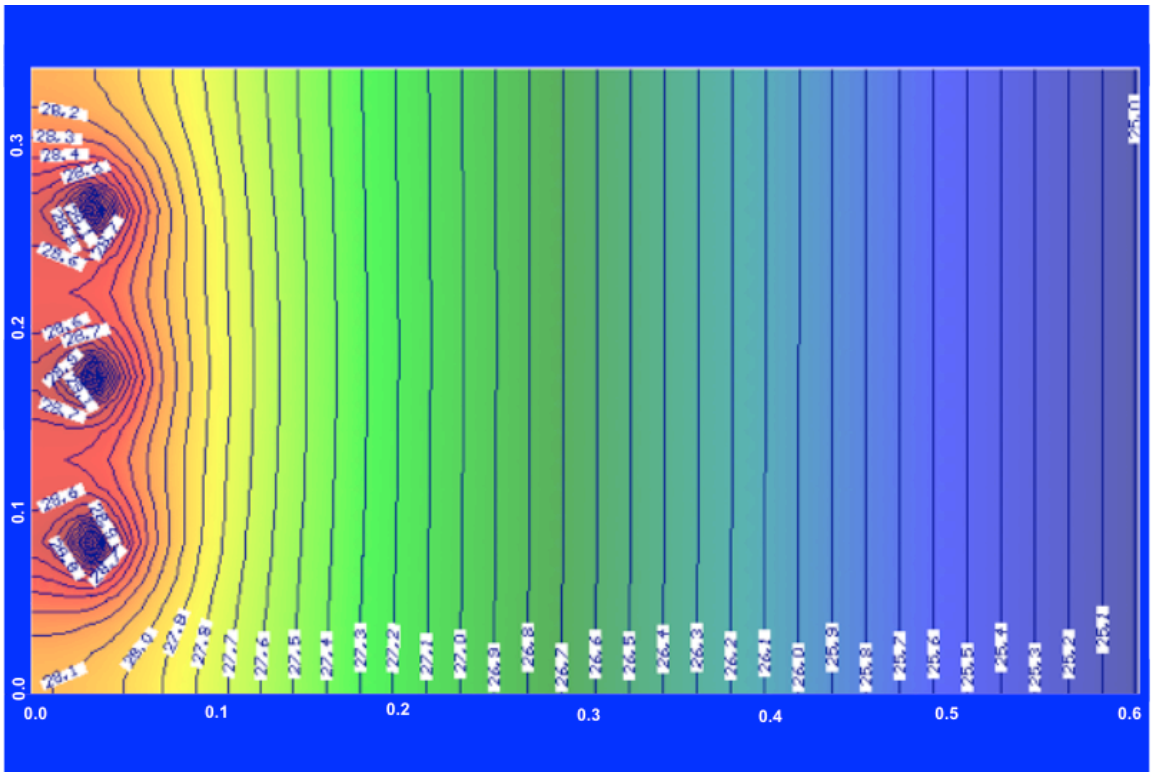

Figure 2.6: Modeled equipotentials associated with flow in a NeST constructed as described in this article. Uniform flow is predicted to occur within 10 cm of the inlet end of the porous medium compartment. The units in the x and y directions are meters.

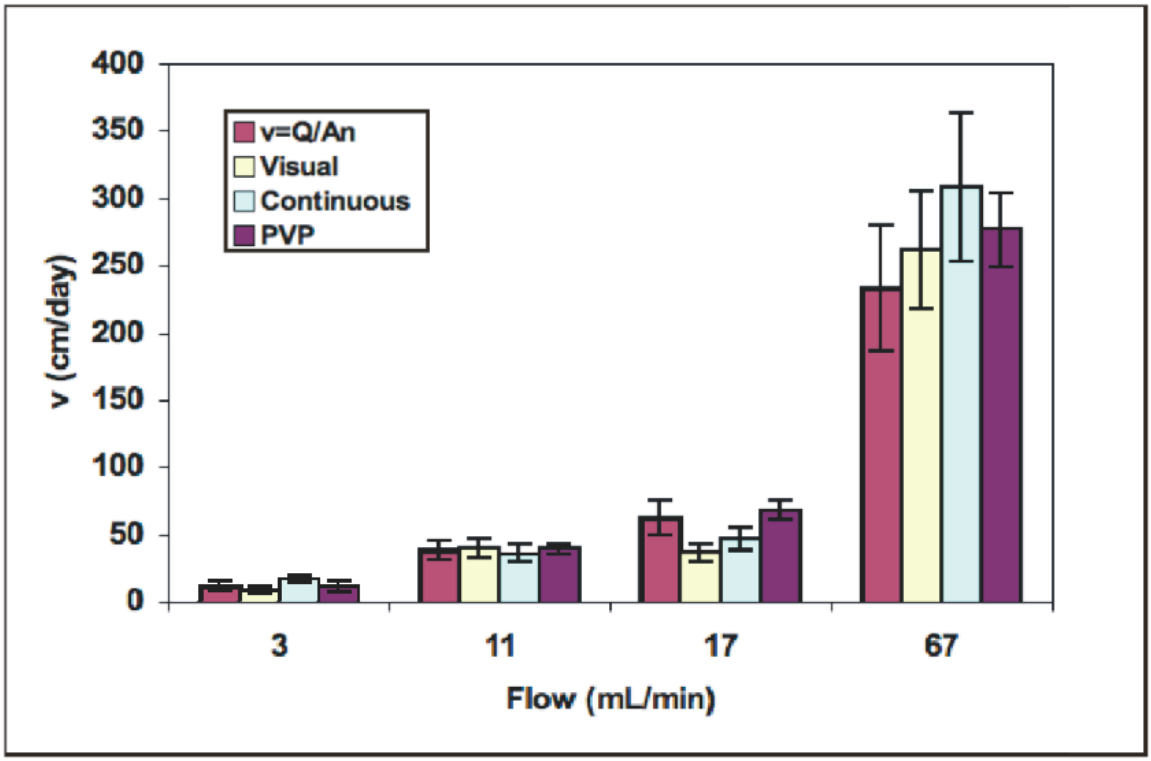

Figure 2.7: Comparison of velocity estimates using the four techniques discussed in the text. The uncertainty represents the relative standard deviation of each technique and flow rate.

Chapter 3.

Development and Laboratory Testing of a Mini-PVP

3.1 Introduction

Detailed site characterization is highly desirable, and sometimes absolutely necessary, to understand and solve hydrogeologic problems associated with groundwater contamination. The effort is often aimed at determining groundwater velocity through direct or indirect means (Ballard 1996; Gavaskar, 1999; Labaky *et al*., 2007). The transport of contaminants in aquifers is governed by groundwater velocity, and detailed knowledge of it is therefore of great advantage for remediation designs. This is particularly true when passive *in situ* remediation schemes are employed (Gavaskar, 1999; Labaky *et al*., 2007). Furthermore, performance assessment of remediation systems will also benefit from a detailed understanding of the relevant groundwater velocity field.

To facilitate the direct measurement of groundwater velocity in the subsurface, a probe was developed that functions at the centimeter scale (Labaky *et al.*, 2007). The point velocity probe (PVP) measures the velocity of a conservative tracer carried by water around a cylindrical body, and relates it to the velocity of the water in the surrounding formation. A PVP is installed in direct contact with the aquifer and operates without a well. Direct aquifer contact results in a tool that is unaffected by well-bore effects (Labaky, 2004).

At least 3 PVP designs have been described in the literature (Labaky *et al.,* 2009; Schillig *et al.,* 2010; Berg *et al.,* 2010). All have been based on a probe design limited to detecting and quantifying horizontal velocities, and constructed

with approximately 5 cm diameters – requiring still larger borehole diameters during installation. Although these devices have worked quite well in their respective tests, there could be advantages in having smaller diameter PVPs capable of installation in small diameter boreholes and the measurement of vertical velocities for detailed investigations of small aquifer volumes, such as flow around a well screen, or flow near discharge points.

The objective of this project was to extend the previous work with PVPs by developing and testing a small PVP capable of measuring vertical and horizontal flow without sacrificing measurement accuracy or precision.

3.1.1 Conventional Estimation of Groundwater Velocity

Velocity is commonly estimated using Darcy's law (Fetter, 2001). The method involves determining the gradient at the site by measuring the hydraulic head and combining the gradient information with hydraulic conductivity and porosity estimates in the following equation

$$\nu = \frac{q}{n} = \frac{K}{n}\frac{\Delta h}{\Delta l} \qquad [1]$$

where ν is the average linear groundwater velocity (Length / Time), q is the specific discharge (Length / Time), n is the porosity (dimensionless), K is the hydraulic conductivity (Length / Time), h is the hydraulic head (Length), and l is the distance over which the hydraulic head is observed to change (Length). A notable limitation of this technique is that its accuracy depends upon the accuracy of the aquifer K, a parameter well known to be highly variable (Ballard, 1996; Butler, 1997). K estimates are also known to be functions of the scale over

which the tests that generate them are conducted (Rovey and Cherkauer, 1995; Schulze-Makuch *et al*., 1999*;* Gierczak *et al.,* 2006; Niemann and Rovey, 2009) because it can vary orders of magnitude over short distances. This variability has been documented even in relatively homogeneous aquifers (Sudicky, 1986). In areas where the hydraulic gradient is small due to short distances between measurements or a prolific aquifer, velocity estimates using Darcy's law may not be reliable (Devlin and McElwee, 2007).

Velocity can be determined through a variety of direct measurement techniques. A common approach is to inject a tracer into the subsurface and monitor its progress through the aquifer. The breakthrough of a tracer at monitoring wells can be used to determine the average groundwater velocity between the injection point and the monitoring points during the time of the test. This method is well established, but is also very time consuming and often requires an extended sampling effort to collect the data (Sudicky, 1986; Hess *et al.,* 2002). Furthermore, tracer tests of this kind only provide spatially averaged velocities with questionable relevance to the velocities associated with features smaller than the scale of the tracer test.

The importance of groundwater velocity estimates and the limitations associated with tracer tests have led to the development of several technologies to measure groundwater velocity directly. Many of these technologies are tracer dependent. Some devices are deployed in wells, such as the colloidal boroscope, borehole dilution, and the Geoflow® meter, (Drost, *et al.,* 1968; Kerfoot and Massard, 1985; Kearl, 1997; Momii *et al.,* 1993; Labaky *et al.*, 2009).

Installation in wells allows for many locations to be tested repeatedly with little installation cost, provided the wells are pre-existing. However, local flow distortion associated with flow through a filter pack and well screen must usually be taken into account with empirical calibrations. Also, well development plays a critical role in the accuracy of the estimated velocity. Finally, these techniques are only capable of measuring the horizontal component of flow and therefore are not useful in three-dimensional aquifer characterization (Ballard, 1996).

Velocity can also be measured directly without a well. The Hydrotechnics VECTOR® Groundwater Flowsensor, also known as the *In Situ* Permeable Flow Sensor (ISPFS), operates by installing a dedicated probe in direct contact with the aquifer. The velocity is determined by monitoring the temperature distribution around the probe, which consists of a heated cylinder. The technique can determine velocity in three-dimensions, however Su *et al.* (2006) suggested that vertical velocity data collected with the VECTOR® Flowsensor may be incorrectly interpreted if the thermal conductivity of the formation is not homogeneous. Additionally, the VECTOR® probe is 0.75 m long and therefore measures flow over a scale that may sample more than one stratum (Ballard, 1996).

3.2 Materials and Methods

The version of the PVP developed in this work was constructed from a cylindrical gas diffusion stone obtained from a pet supply store. The stone was painted with a concrete sealant leaving a small hole (~ 5 mm) uncovered to act as the injection point for the tracer release. Stainless steel wire pairs, making up

the conductivity detectors, were spaced 2-3 mm apart and affixed to electrical tape, which was placed on the probe surface in the desired locations. Six pairs of 0.018" diameter stainless steel wires were used in the current designs (Figure 3.1). The entire stone, with the exception of the injection port and the detector wires, was then coated with epoxy cement to ensure a well-sealed, smooth probe body and secure detector wires. The detector wires were connected to a 12-conductor cable using heat-shrink butt connectors to transmit the signal to the surface. The diffusion stone was connected to an injection line that carried the tracer from an injection system consisting of a 60-mL reservoir syringe and a 1-mL injection syringe (Figure 3.1).

The detector system operated by measuring changes in resistance of the water as the tracer passed over the detector wires (Devlin *et al.,* 2009*)*. Two detectors for measuring horizontal velocity were placed on each side of the injection port, and two more wire pairs were placed above and below the injection port to detect vertical flow (Figure 3.1). The breakthrough of the tracer at each detector was used to calculate an apparent velocity (v_{app}). These were used to determine the average linear velocity locally in the aquifer (v_{∞}), and the orientation of the injection port with respect to that groundwater flow direction (α) as seen below (Labaky *et al.*, 2007). Generally, the angle α was estimated first from the following relation,

$$\alpha = \tan^{-1}\left[\frac{\nu_{app1}\gamma_1(cos\gamma_2 - 1) + \nu_{app2}\gamma_2(1 - cos\gamma_1)}{\nu_{app1}\gamma_1 sin\gamma_2 \; - \nu_{app2}\gamma_2 sin\gamma_1}\right] \qquad [2]$$

where v_{app1} and v_{app2} are the apparent velocities for detectors 1 and 2, respectively. The angle between the injection port detector 1 is γ_1, and γ_2 is the

angle between the injection port and detector 2. These angles were fixed at 40° and 70°, respectively, in the current PVP design. After determining α, the average linear groundwater velocity was determined using an apparent velocity from either detector and the relationship (Labaky *et al.*, 2007),

$$\nu_{\infty} = \frac{\nu_{app}\gamma}{2(cos\alpha - cos(\alpha+\gamma))} \quad [3]$$

where ν_{∞} is the average linear groundwater velocity. In the case of the vertical velocity, the apparent velocity (ν_{app}) was assumed equal to the average linear velocity in the vertical direction because the probe surface was not curved in that direction.

3.3 Experimental Procedure

The probe was tested in the laboratory using an inexpensive flow-through tank called the Nested Storage Tank, hereafter referred to as the NeST (Figures 2.1 and 2.3) (Chapter 2). The probe was placed in the center of the NeST, which was then wet-packed with sand. This packing procedure ensured near uniform packing of the sand and eliminated measurement biases that might have resulted from disturbance of installation in pre-packed sand. All tests were conducted in medium sand obtained commercially. A porosity of 0.52 ± 0.13 was determined gravimetrically. The tracer solution consisted of a 1 g/L NaCl solution to ensure conductivity was higher in the tracer solution than in the background tap water.

A test began with the injection of a pulse of tracer (0.2 mL was typical) using the small syringe in the injection system; the larger syringe was used to

recharge the smaller one in subsequent tests. The conductivity at the detectors was monitored every 10 to 60 seconds depending on the anticipated average linear velocity in the test. The device was assessed over the velocity range 12 to 625 cm/day, and with the α angle varying from 0° and 120°. The results of the tests were compared to a calculated velocity estimated from,

$$\nu = \frac{Q}{An} \qquad [4]$$

where *Q* is the discharge of the pump (L^3/T), *A* is the cross-sectional area of the saturated sand (L^2), and *n* is the porosity (dimensionless). All units are generalized, where L is length and T is time. The direction of flow was assumed to be perpendicular to the open water columns at either end of the tank.

Breakthrough curves were obtained from each detector and were used to estimate the apparent velocities needed for equations 2 and 3. This was done by fitting the data with a 1-D solution to the advection-dispersion equation, using simplex optimization algorithm coded in a visual basic application (VelprobePE) (Devlin, 1994; Schillig, 2010)

3.4 Results and Discussion

The precision of PVP measurements was assessed by making several measurements in sequence under identical conditions. This assessment was repeated at several pumping rates with results similar to those reported for earlier PVP designs (Table 3.1) (Labaky *et al.,* 2007). Also, breakthrough curves from any 2 consecutive measurements were generally found to be nearly identical

(Figure 3.2). These results confirm the inherently high precision of the PVP instrument.

The PVP was further assessed by comparing PVP-derived velocities to those estimated by other means, over a wide range of velocities. In most experiments, PVP velocities could be compared with velocities calculated using equation 4. These comparisons usually showed very good agreement (Figure 3.3). It should be noted that velocities from equation 4 depend upon good estimates of porosity, which was determined empirically to be within the range 0.38 to 0.65 in the NeST tests using cores from the NeST and beakers wet packed in a fashion similar to that employed in packing the NeST. Thus, the large uncertainty in porosity can account for much or all of the discrepancies that existed between the PVP measurements and the equation 4 velocity estimates.

The accuracy of the PVP velocities also appeared to be very good, with velocities agreeing to within 20% in all but one test (Table 3.2). The results of the tests at α = 60° show the highest deviations in both magnitude and direction from Q based velocities. The reason(s) for these disagreements are not known for certain, but those specific tests were conducted in a tank packed separately from the other tests, and were conducted out of sequence with the other tests. This raises the possibility that the anomaly is due to differences in the tank conditions rather than any error inherent in the method. If this anomalous test is excluded, the results with the highest error in magnitude are those with α = 90° or greater, corresponding to the 2nd detector being rotated into or near a stagnation point on the probe surface, i.e., at. $\alpha = 180^{o}$ (Di Biase, 1999; Labaky, 2004).

The α angle was measurable with reasonable accuracy, ~ ± 15°, over the velocity range 11 to 294 cm/day (Table 3.2). The best results in terms of accuracy and precision were obtained for the higher flow velocities. This might be related to difficulties in maintaining constant flow rates from the pump at the lowest tested velocities. Nevertheless, these data suggest that the uncertainty in PVP flow directions is likely less than ± 15°, and the average error was ± 8°, consistent with previous assessments for earlier designs (Labaky *et al.,* 2007).

The PVP was further evaluated by comparing its velocity estimates to those from two tracer tests (Table 3.3). The tracers included both a dye tracer and a chemical tracer. The dye was used to conduct a test in which the tracer could be tracked visually. Blue food coloring was applied to the saturated sand surface near the inlet end of the tank. As water flowed through the tank, tracer was transported at the same rate and was timed as it arrived at predetermined points in the tank.

The chemical tracer test was performed by adding sodium chloride to the tank inlet water to raise its concentration to 1 g/L, creating a prolonged high conductivity pulse that was tracked with electrical conductivity sensors installed in the tank.

Both tracer tests returned velocity values that were in close agreement with the PVP velocities, further indicating the PVP probe provided accurate estimates of velocity. At the highest velocities (~233 cm/day), the PVP-measured velocities deviated from the equation 4 estimates by about 25%. However, the results from the other tracer tests were in good agreement with the

PVP, suggesting that the error was with the equation 4 values rather than the measurements.

Finally, the PVP performance was directly compared to the performance of an older design PVP with a larger diameter, using the methods previously described (Labaky *et al.,* 2007). The two PVPs produced similar velocity estimates, although the smaller instrument's estimates were consistently lower in value than the larger instrument estimates by about 20% on average (Appendix D). The reasons for the apparent bias bear further investigation. For the present, it is hypothesized that they are due to small variations in porosity across the tank, which would have been continuously present throughout the tests. Alternatively, it is possible that the smaller PVP was sensitive to heterogeneities in the packing at a smaller scale than the larger PVP.

As mentioned above, a goal of the PVP design introduced in this work was to characterize flow in 3-dimensions. This was accomplished by adding vertical flow detectors to the probe. The ability to detect vertical flow was tested in the laboratory by orienting a PVP on its side and following the same testing procedure described above (Figure 3.4). The work presented here is preliminary and more work should be pursued in the future. However, the results suggest good accuracy and precision relative to the horizontal flow capability (Table 3.4).

3.5 Conclusions

Laboratory testing of a new PVP design showed that it is capable of providing precise and accurate estimates of velocity magnitude in sandy

deposits. The velocity magnitudes agreed within 20% of other mini-PVP measurements and within 25% of other velocity estimation techniques. The α directions had an average uncertainty of 8°. These uncertainties are consistent with other PVP designs. However, the mini-PVP measured velocities were consistently less than the larger PVP estimates. The cause of the bias is unknown, but the accuracy and precision suggest the mini-PVP design is expected to perform as well as the larger design in sandy material. Additionally, the mini-PVP may be used to map complicated 3-dimensional flow systems such as those created around a dipole well or other systems with strong components of horizontal and vertical flow.

Table 3.1: Individual PVP tests reported with expected values for alpha and speed. These results show the reproducibility of measurements made with a PVP. The uncertainty represents the average uncertainty for each measurement.

Discharge (mL/min)	Expected Alpha (Degrees)	Measured Alpha (Degrees)	Expected Speed (cm/day)	Measured Speed (cm/day)
3.5 ± 0.1	40 ± 5	79 ± 8	14 ± 3	16 ± 2
2.3 ± 0.1	40 ± 5	61 ± 8	9 ± 2	4 ± 1
4.0 ± 0.1	40 ± 5	37 ± 8	16 ± 4	13 ± 2
4.1 ± 0.1	40 ± 5	31 ± 8	16 ± 4	14 ± 2
3.3 ± 0.1	40 ± 5	68 ± 8	13 ± 3	12 ± 2
11.0 ± 0.1	40 ± 5	24 ± 8	44 ± 10	37 ± 6
12.0 ± 0.1	40 ± 5	35 ± 8	48 ± 11	42 ± 6
10.6 ± 0.1	40 ± 5	28 ± 8	43 ± 10	38 ± 6
10.4 ± 0.1	40 ± 5	23 ± 8	42 ± 10	40 ± 6
17.0 ± 0.1	40 ± 5	27 ± 8	68 ± 16	59 ± 9
18.0 ± 0.1	40 ± 5	25 ± 8	72 ± 17	73 ± 11
18.2 ± 0.1	40 ± 5	28 ± 8	73 ± 17	71 ± 11
18.0 ± 0.1	40 ± 5	25 ± 8	72 ± 17	69 ± 11

Table 3.2: Summary of PVP Assessments Using a Laboratory Tank. The absolute error is reported.

		Velocity Magnitude		Velocity Direction		Error	
Alpha	No. of Replicates	Expected (cm/day)	Measured (cm/day)	Expected (deg)	Measured (deg)	Magnitude (%)	Direction (Degrees)
0	2	261	267	0	8.8	2.6	-8.8
20	2	248	251	20	20.0	1.2	0.0
30	2	104	99	30	30.1	-5.1	-0.1
30	3	225	230	30	27.4	2.2	2.6
30	3	626	624	30	20.9	-0.4	9.1
40	5	14	12	40	55.1	-15.2	-15.1
40	4	44	39	40	27.6	-11.3	12.4
40	4	71	68	40	26.7	-4.9	13.3
40	2	248	294	40	31.7	18.4	8.3
60	2	253	360	60	80.8	42.4	-20.8
70	4	255	285	70	68.2	11.7	1.8
80	2	249	293	80	84.8	17.9	-4.8
90	2	249	344	90	99.6	38.2	-9.6
100	2	245	315	100	N/A	28.5	N/A
110	2	253	293	110	N/A	16.0	N/A
120	2	251	311	120	N/A	24.1	N/A

Table 3.3: Comparison of PVP velocities with tracer tests. The uncertainty represents the error associated with one standard deviation for each measurement.

Approximate Pump Rate (ml/min)	Velocity (From equation 1) (cm/day)	Visual Tracer (cm/day)	Chemical Tracer (cm/day)	Point Velocity Probe (cm/day)
3	12 ± 4	8 ± 3	17 ± 0.3	12 ± 4
11	38 ± 8	40 ± 7	36 ± 7	39 ± 2
17	62 ± 12	36 ± 3	46 ± 5	68 ± 6
67	233± 48	261 ± 20	308 ± 7	277 ± 23

Table 3.4: Summary of Vertical Velocity Data. The uncertainty represents the average uncertainty for the PVP and expected velocity.

Discharge (ml/min)	Expected Velocity (cm/day)	PVP Velocity (cm/day)
45	186 ± 37	177 ± 27
45	186 ± 37	170 ± 26
43.5	180 ± 36	178 ± 27
43.5	180 ± 36	173 ± 26

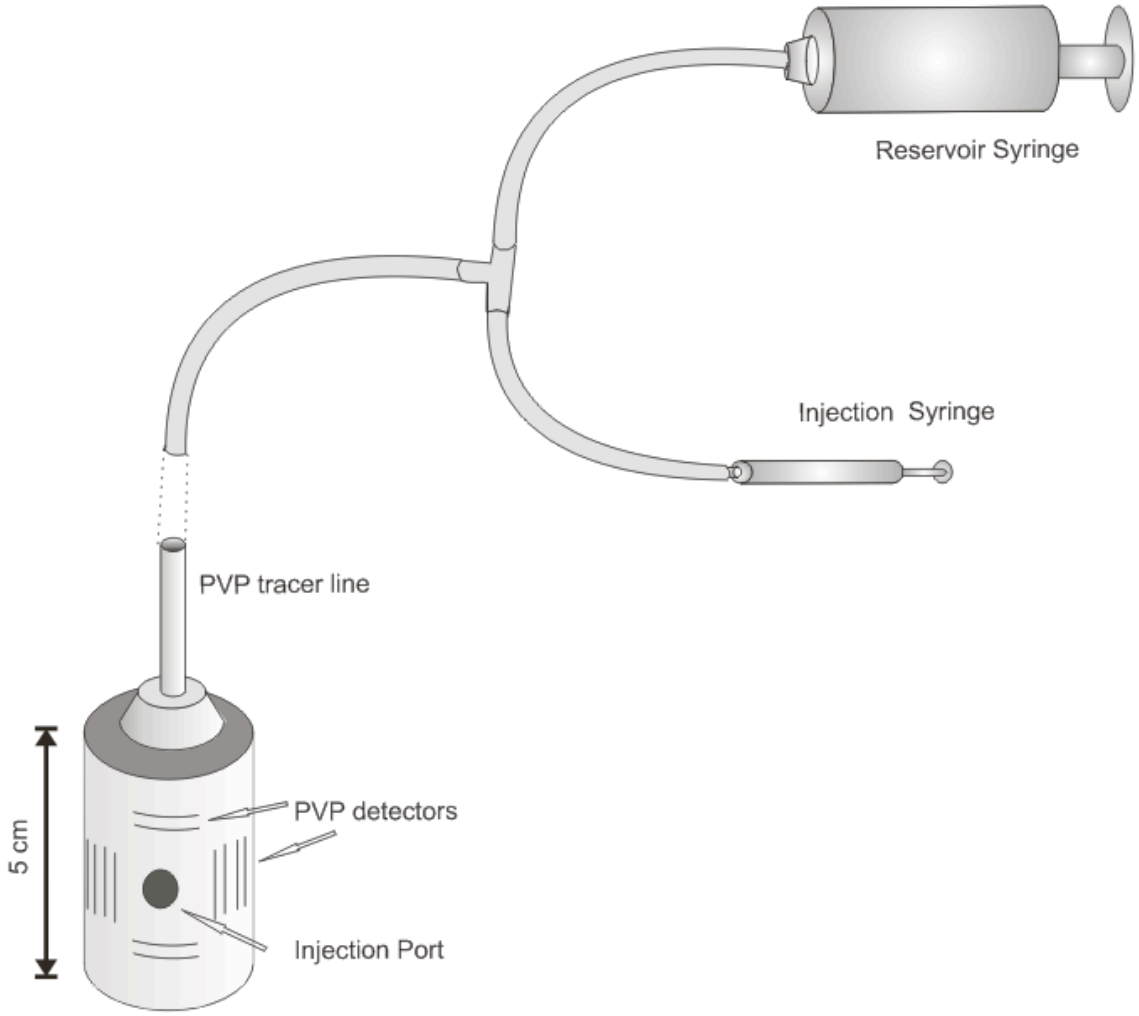

Figure 3.1: Schematic of mini-PVP showing injection port, detector, and tracer injection system.

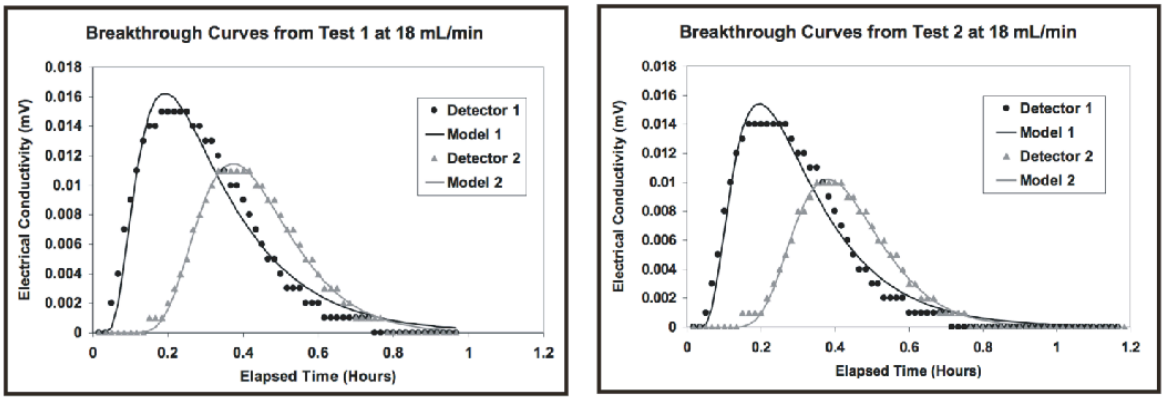

Figure 3.2: Comparison of PVP breakthrough curves from tests conducted under identical conditions. Symbols represent data collected from the PVP detectors and lines represent best fit solutions to the advection dispersion equation (see text). In consecutive tests like these the curves produced were nearly identical.

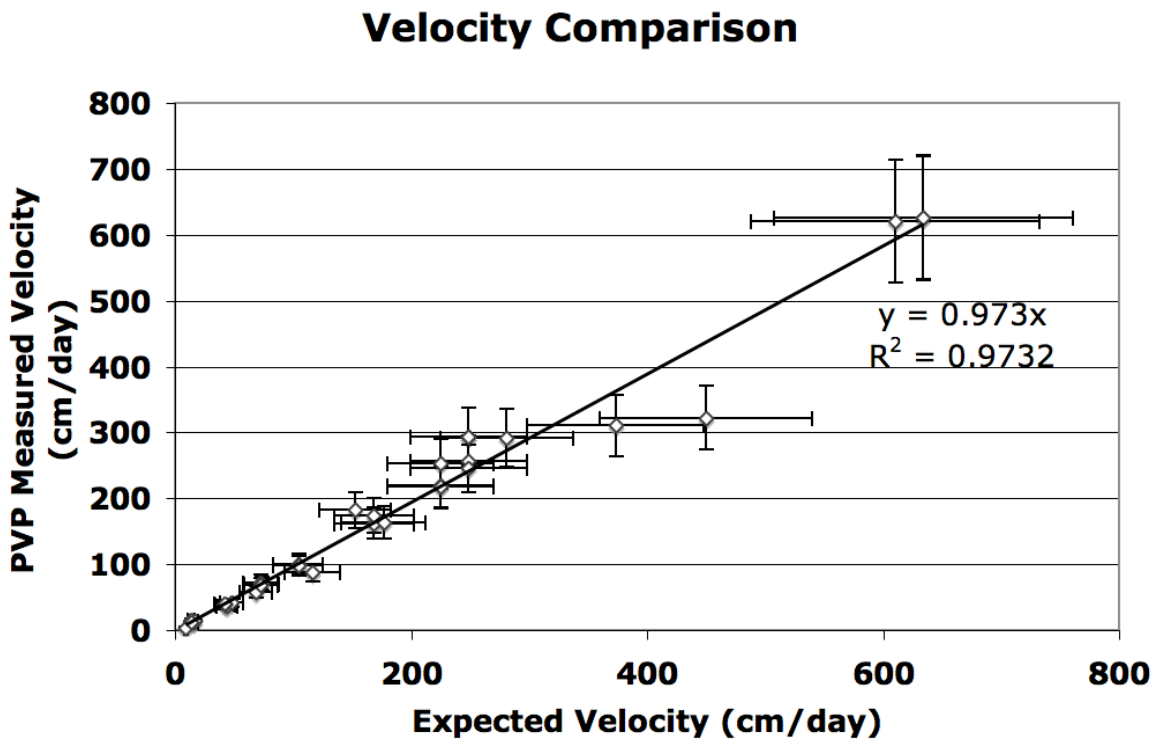

Figure 3.3: Agreement between velocities measured with the PVP and the expected velocity calculated using equation 3. Note the slope is very near 1 indicating good accuracy. The horizontal error bars represent the error in expected velocity as a result of the uncertainty in the pumping rate, porosity, and cross sectional area. These errors combined result in an average uncertainty in the equation 4 velocity estimates of 23%. The vertical error bars represent 15% uncertainty, which is the average uncertainty in magnitude for the PVP.

Figure 3.4: Photo depicts PVP orientation when testing vertical flow detection.

Chapter 4.

Velocity Characterization of the Dipole Flow and Reactive Tracer Test

4.1: Introduction

The remediation of contaminated groundwater is dependent upon an accurate understanding of the affected aquifer. Therefore, site characterization is a crucial step in any effective remediation system. The need for many different types of site-specific information has led to the introduction of a number of characterization techniques and tools. One of the most important parameters to determine is groundwater velocity (Gavaskar, 1999). The Point Velocity Probe (PVP) was developed to address this need. A PVP measures groundwater velocity directly by relating the velocity in the formation to the velocity of a conservative tracer on a cylindrical probe surface (Labaky *et al.*, 2007).

PVPs are installed in direct contact with the aquifer porous medium, and operate without a well. This ensures that the velocity measured is unaffected by well screens and well bore effects. The tool measures groundwater velocity at the centimeter scale, which makes high-definition characterization of complicated flow systems possible. In this study, the probe is used to provide velocity information around a dipole flow system.

Dipole flow systems are the basis for a number of site characterization and remediation schemes. These systems, also known as groundwater circulation wells, have been used to deliver surfactants, oxidants, and nutrients for bioremediation in order to improve remediation performance (Phillip and Walter, 1992; Knox *et al.,* 1997; Sabatini *et al.,* 1997). Dipole Flow Tests can be

used to determine vertical and horizontal *K* and specific storativity of porous media (Kabala, 1993). Recently, the Dipole Flow Test has been combined with a suite of tracers to determine other aquifer properties, related to contaminant fate and transport, in a test called the Dipole Flow and Reactive Tracer Test, DFRTT (Thomson *et al.,* 2005).

The DFRTT is capable of determining a number of physical, chemical, and biological aquifer parameters from a single test. The device uses packers to isolate two portions of a well screen. Water is injected into the formation from one screen and pumped out from the other, using a pump located at the surface. The pressure in each chamber, and the tracer concentrations, are monitored over time and used to determine the various aquifer parameters. It is the tracer breakthrough curves (BTCs) that were of particular interest in the DFRTT research because they could be used to estimate aquifer parameters such as microbial activity, aquifer sorption properties, and contaminant degradation rates (Roos, 2009). However, the preliminary DFRTT modeling, which assumed an homogeneous aquifer and no significant ambient groundwater flow, was unable to accurately reproduce the tracer breakthrough curves. It has been shown in tank experiments that even small-scale heterogeneities can affect the tracer BTCs of DFRTTs (Barns *et al.,* 2010). The possible deviations from ideal BTCs include multiple tracer peaks that are usually attributed to a combination of short-circuiting along the well casing, and the expected BTC. Other differences arise in the magnitudes of peak concentrations, time-to-peak concentration, and different shapes of the BTC tails (Figure 4.1).

In this study, PVPs were used to evaluate the flow system surrounding an operating dipole well in unprecedented detail. The primary objective of this work was to identify causes of the disagreements between modeled and measured BTCs by defining the groundwater velocity field at steady state near the dipole well. Attempts have been made to measure velocities near a dipole flow system in other work (Johnson and Simon, 2007). However, those studies used VECTOR® Technology instrumentation (Ballard, 1996) that averaged velocity measurements over a vertical distance of nearly a meter, and the instrument was unable to measure vertical velocities – information crucial to properly characterizing flow around a dipole well (Johnson and Simon, 2007). That study found that horizontal velocity estimates generally agreed with model estimates, but the agreement was not entirely satisfactory. In this work, we extend the previous efforts by improving the resolution of the measurements and adding vertical velocity measurements to the data collected. To accomplish this, PVPs were redesigned and deployed around a dipole well previously investigated by Thomson *et al.* (2005).

A secondary objective of this work was to evaluate the magnitude of flow short-circuiting along the well casing, and to assess the effect this might have on the tracer BTCs.

4.2 Site Description

The study site was located 80 km northwest of Toronto, Ontario at Canadian Forces Base (CFB) Borden. The aquifer consisted of well-sorted fine to medium sands of a glacio-lacustrine deposit and was interbedded with peat in

some areas (Macfarlane, 1983; Brewster *et al*., 1995), and fine horizontal beds that were visible in core. The aquifer was underlain by a silt and clay aquitard approximately 9 m below ground surface (bgs) (MacFarlane *et al.*, 1983).

The site is uncommonly well characterized and the aquifer has been evaluated for *K* many times, using a variety of techniques. For example, constant head permeameter tests of core material resulted in an average *K* of 8.0 x 10^{-5} m/s for homogenized 5-cm samples of core material (Sudicky, 1986; Woodbury *et al.*, 1991). Intact core material was also studied with a mean *K* of 2.6 x 10^{-5} m/s (Tomlinson *et al.*, 2003). Slug test estimates had a mean *K* of 2.5 x10^{-5} m/s but individual measurements varied from 3.8 x10^{-6} to 6.1 x10^{-5} m/s. Pumping tests, which tend to sample larger volumes of aquifer than the other methods, returned *K* estimates that were notably greater than those from the other techniques. The results ranged from 1.4 x10^{-4} to 2.2 x10^{-4} m/s (Nwankwor *et al.*, 1984). These mixed results show that even in a relatively homogeneous aquifer the *K* can vary over nearly two orders of magnitude, and is scale dependent. This variability can compound the uncertainties associated with indirect velocity-estimation methods, like those based on Darcy's Law calculations (Labaky *et al.,* 2007).

4.3 PVP Construction and Theory

The Point Velocity Probe operates by tracking the movement of a tracer around a cylindrical body. The version of the device developed for this project was constructed from a cylindrical diffusion stone. In order to constrain the tracer

injection to a small area on the cylinder, the stone was painted with a concrete sealant leaving only a small opening. Following sealing, the detectors, consisting of 12 stainless steel wires (0.018" in diameter) in six pairs were secured to the stone with tape (Figure 3.1). Two detectors for measuring horizontal velocity were placed on each side of the injection port, and one detector was placed on each side of the injection port vertically. The entire stone was then coated in epoxy cement leaving only the wires and injection opening – now the injection 'port' – exposed. The wires were connected to a 12-conductor 20-gauge copper cable using heat-shrink butt connectors. The cable connected the probe to a datalogger through a half-bridge circuit that returned millivolt signals proportional to electrical resistance of the groundwater (Devlin *et al.,* 2009). The probe was connected to an injection line for the delivery of tracer by a user. Tracer delivery was controlled with a 60-mL reservoir syringe and a 1-mL injection syringe (Figure 3.1).

The peak amplitudes of the electrical resistance of groundwater at each detector represented the maximum tracer concentrations and were used to calculate the apparent velocity (ν_{app}) of tracer moving around the probe. The procedure involved fitting tracer breakthrough curves at the detectors with a solution to the 1-D advection-dispersion equation. The system was automated so that signals from multiple detectors could be processed in a single user step. This was accomplished by coding the fitting procedure into visual basic, within Excel®, in an application named VELPROBE PE (Schillig, 2010, Devlin, 1994). The apparent velocities from two detectors were used by VELPRBOBE PE to

determine the orientation of the injection port with respect to the groundwater flow direction (α) as seen below (Labaky *et al.*, 2007):

$$\alpha = \tan^{-1}\left[\frac{\nu_{app1}\gamma_1(cos\gamma_2 - 1) + \nu_{app2}\gamma_2(1 - cos\gamma_1)}{\nu_{app1}\gamma_1 sin\gamma_2 \; - \nu_{app2}\gamma_2 sin\gamma_1}\right] \quad [1]$$

where ν_{app1} and ν_{app2} are the apparent velocities for detectors 1 and 2, respectively. The angle between the injection port and detector 1 is γ_1, and γ_2 is the angle between the injection port and detector 2. For the PVPs used in this study, these angles were fixed at 40° and 70° respectively. After determining α, the average linear groundwater velocity was calculated by VELPROBE PE from (Labaky *et al.*, 2007):

$$\nu_\infty = \frac{\nu_{app}\gamma}{2(cos\alpha - cos(\alpha + \gamma))} \quad [2]$$

where ν_∞ is the average linear groundwater velocity. In the case of detectors oriented to measure vertical velocities, the apparent velocity (ν_{app}) was assumed equal to average linear velocity because the tracer path was straight (no cylinder curvature) between those detectors and the injection port.

4.4 PVP and Well Installation

The well used to create the dipole flow system (MW-3) was a 5.1 cm inside diameter (ID) PVC well installed to a depth of 5.5 m bgs and completed with a 3 m long 0.010" slot screen. The well was installed by driving a 7 cm ID hollow steel casing into the aquifer and then flushing the casing with water to remove the sand. After flushing, the PVC well was placed inside the casing, which was subsequently removed allowing the aquifer material to collapse

around the well screen and riser pipe. This method of installation is known as 'jetting' and has the advantage of creating a well bore with the least possible disturbance of the surrounding aquifer material (Labaky, 2009).

Additional wells were installed with the purpose of permitting an evaluation of short-circuiting along the well casing during pumping. In these cases, the riser pipes located between the two screens were fitted with PVP-type detectors to measure vertical tracer velocities along the well body (Figure 4.2). In order to evaluate the effect of a filter pack on short circuiting, one well, MW-A, was constructed with a 1.5 m screen and installed to a depth of 5.5 m, as described above. A second well, MW-B, similarly constructed, was installed with a filter pack. The filter pack was created by jetting a larger steel casing (13 cm ID) and filling the annulus around the well with the pack material.

The PVPs were constructed as described above in the section titled PVP Construction and Theory. They were mounted onto 1" PVC riser pipes and installed by jetting using a 3.8 cm ID hollow steel casing with no filter pack. Altogether, 18 probes were deployed at 3 different distances and depths surrounding MW-3 (Figure 4.3). The horizontal distances were chosen to fully characterize the flow system in an effort to explain the BTC deviations from the DFRTT model (Figure 4.1). Preliminary modeling using MODFLOW was used to decide placement of the PVPs so the innermost PVPs would record flow within the 70% cumulative flow boundary.

The depths of monitoring were chosen to provide a detailed three-dimensional image of the dipole flow system in the vicinity of the pumping and extraction screens, which were centered at 4.9 m bgs.

4.5 Dipole system

A downhole device, hereafter referred to as the dipole packer assembly (DPA), developed at the University of Waterloo, was used to create the dipole flow system in this investigation (Figure 4.2) (Roos, 2009). It consisted of 3 inflatable rubber packers that were used to isolate the injection and extraction chambers. The DPA had the characteristic dimensions L = 0.22 m and Δ = 0.079 m (Figure 4.2). These measurements are important when discussing the area of influence of the dipole well, where 70% of flow occurs within the region bounded by 3L (Kabala, 1993; Zlotnik and Zurbuchen, 1998). The DPA also contained two pressure transducers (Huba Control, Type 680) that were mounted in the upper and lower packers, and connected to the chambers with stainless steel tubing. The pressure transducers were monitored with a data logger and used to determine steady state flow conditions. A peristaltic pump (Cole Parmer, K-07553-70) was located at the surface and used to induce flow. The surface mounted pump resulted in a smaller DPA design as well as ease in plumbing the other surface equipment (Roos, 2009).

4.6 Field Methodology

4.6.1 Dipole operation

The dipole flow system was created by inserting the DPA into MW-3 such that the mid point between the screens was at a depth of 4.9 m bgs. This depth was chosen because previous dipole experiments returned reproducible results at this well/depth combination (Roos, 2009). After inserting the dipole, the packers were inflated to a pressure of approximately 30 pounds per square inch (PSI). This pressure was sufficient to ensure no short-circuiting of flow through the well bore, inside the well screen. Following packer inflation, the dipole unit was connected to a peristaltic pump at the surface. In these experiments, the pumping rates chosen were ~700 mL/minute and ~1150 ml/minute. The pump was operated from 0.5 (June, 2009 experiment) to 14 hours (September, 2009) before measurements were made to allow the system to reach steady state. In both cases, head measurements made with pressure transducers in the DPA indicated that steady state flow was established within the screen.

4.6.2 Velocity field characterization

In order to characterize the flow system surrounding the dipole well, 18 Point Velocity Probes were installed around it at various depths. Following installation of the PVPs, or after long periods of non-use (>7 days), the PVP lines were flushed with fresh tracer solution. In the first set of experiments, a tracer solution of 1 g/L of NaCl was utilized with success, but signal amplitude was less than desired. To improve detection, the later experiments were conducted with 3

g/L NaCl, which had proven satisfactory in previous field tests (Labaky *et al.,* 2009). After flushing, the resistance measured at the PVP detectors was monitored until it returned to background levels before beginning subsequent tests.

Tests were begun by simultaneously injecting a known volume of tracer at each probe. The volumes chosen were between 0.3 mL and 0.7 mL. The resistivity was monitored for a period of at least 10 hours to ensure that breakthrough in the slowest velocity zones was complete. The datalogger was programmed to record resistivity measurements at 30-second intervals. In experiments utilizing the detectors on the dipole well itself, data were collected at one-second intervals.

4.7 Results and Discussion

In all tests, the field data were marked by a small peak in tracer concentration at early times. This peak has been observed in previous tests and attributed to tracer short-circuiting along the well casing and reaching the extraction chamber earlier than expected (Roos, 2009). Testing was completed to specifically examine this phenomenon (at MW-B), and tracer movement along the casing was confirmed, presumably through a skin of disturbed porous medium at the casing-aquifer contact (Appendix A). The tests showed that the tracer that short-circuited the flow system traveled at unusually high velocities (>8500 cm/day). If correct, the early time peaks effectively mark the start times of the injections, i.e., the times when the tracer entered the formation after the

pump was started. Taking into account the time for the tracer to return to the surface detector through the DPA tubing and intake screen, a conservative delay of 6 minutes was estimated. With this adjustment to the time axis, the small short-circuit peak can be used as a time-zero marker.

Data from the various tests were time corrected as described above to permit the BTCs from the June and September tests, and model simulations, to be directly compared. In addition, all data were normalized to the peak maxima C_{max}, again to facilitate comparisons. These measures had the advantage of enhancing the visual differences in the falling limbs of the tracer BTCs, referred to as the tails (Figure 4.4). The extreme right ends of the tails are associated with the longest flowpaths. Tails can also be extended due to nonideal transport caused by heterogeneities in the aquifer. Sutton *et al.* (2000) suggested that only 10% of the flow from the injection chamber of a dipole well is responsible for the BTC peaks, whereas the remaining 90% of flow controls the shape of the tail.

The DFRTT model assumed an homogenous aquifer, and because heterogeneity was likely to be a primary cause of the disagreement, another model was created, using Visual MODFLOW Pro®, that could introduce heterogeneity as required (Appendix B). In addition, the MT3DMS (Zheng and Wang, 1998) engine was used to model tracer breakthrough. This model was used to simulate all flow and transport in the experiments.

The breakthrough-curve peaks from the first data set (June 2009) arrived earlier than predicted by the Visual MODFLOW Pro® model and earlier than observed in the previous tests (Figure 4.4). In all cases, the tails of BTCs from

the experiment declined more quickly than observed in earlier tests (Figure 4.4). This suggested that the tracer mass was returning to the intake screen along shorter and/or faster flowpaths than would be present in an homogeneous aquifer. The PVP velocity data were used to evaluate the likelihood of this interpretation.

A projected cross section of the PVP results was compared to the homogeneous model created in Visual MODFLOW Pro® (Figures 4.5). The results show good qualitative agreement in velocity magnitude and direction. Generally, water was flowing away from the well near the injection screen (measured with the shallow PVPs) and toward the well near the extraction screen (measured with the deep PVPs). Furthermore, flow was downward at the mid-depth PVPs (4.9 m bgs), as expected in a dipole system. Despite the generally good agreement between the modeled and experimental data sets, some location-specific disagreements were observed. This was particularly evident at the shallowest PVPs, where some of the measurements indicated a notable upward component of flow instead of dominantly horizontal flow, as predicted by the model. The magnitudes of the measured velocities also showed some deviations from the MODFLOW® modeled velocities. Experimental velocities were higher near the well than those predicted by the model (Figures 4.5 and 4.6). Outside the region of fast flow some of the velocities were lower than model predictions. These results suggest that the area of influence of the well may have been smaller than predicted and that local heterogeneities may have contributed to these differences. Hydraulic conductivity profiling with the dipole

assembly, using the equations of Zlotnik and Zurbuchen (1998), showed variations in *K* with depth that support this possibility but fall short of defining a *K* field that could explain the BTC discrepancies (Figure 9). However, the velocity differences detected by the PVPs were sufficient to begin altering the model to match the field data.

To improve the agreement between modeled and measured velocities, the aquifer was treated as a layered system in MODFLOW®. Simulations were conducted in which the *K* profile from Figure 4.7 was used to define a continuous zone extending across the entire domain with a *K* of 3.87 x 10^{-5} m/s near the injection screen and 5.8 x 10^{-5} m/s above and below the stratum (based on an average *K* from the dipole tests) (Figure 4.8 A). In another simulation, a high-*K* stratum (*K* = 5.8 x 10^{-5} m/s) between the injection and extraction chambers was assumed, while the surrounding formation had a lower *K* (*K*=3.87 x 10^{-5} m/s) (Figure 4.8 B), and in yet another simulation a continuous low-*K* layer (*K* = 3.87 x 10^{-5} m/s) at the depth of the extraction chamber was simulated while the surrounding formation had a *K* of 5.8 x 10^{-5} m/s (Figure 4.8 C). In all cases, these simulations tended to cause only small changes in arrival times and peak concentrations of the tracer at the extraction chamber compared to the homogeneous aquifer simulations (Figure 4.8). The nature of the trends agreed with expectations from tank experiments (Barns *et al.*, 2010), but the magnitudes of the changes were too small to explain the experiment-model differences. It was concluded that only heterogeneities in the immediate vicinity of the dipole

well were likely to influence calculated breakthrough curves enough to force a match between the modeled and measured data sets.

The PVP velocities were higher than predicted near the well, suggesting that aquifer was generally more permeable there than further away. Therefore, simulations were performed based on the assumption that *K* within 0.4 m from the well was relatively higher than elsewhere (Figure 4.9). This simulation did not achieve the desired convergence in measured and modeled BTCs (Figure 4.8D). However, the presence of a hypothetical zone with higher *K* even nearer (0.1 m radial) to the dipole well (K = 8.7 x 10^{-5} m/s near the well and K=5.8 x 10^{-5} m/s at distance) resulted in changes in the simulated BTCs in the direction of the field data (Figure 4.10A). Proximal zones of lower *K* were also considered (*K* = 1.93 x 10^{-5} m/s near the well and K=5.8 x 10^{-5} m/s at distance) and found to result in simulated BTCs with broader, lower peaks, and longer tails than the previous homogeneous aquifer simulations (Figure 4.10B). This series of simulations showed that indeed heterogeneities immediately next to the dipole well were likely dominating the experimental BTCs.

Finally, an attempt was made to quantitatively reduce the discrepancy between simulated and experimental BTCs. A small proximal zone of aquifer with a *K* of 6.5 x 10^{-5} m/s was placed near the well (0.1 m) and the rest of the aquifer was assigned a *K* of 5.8 x 10^{-5} m/s. This scenario resulted in an improved match between the modeled and measured BTCs, as desired (Figure 4.11). The match could be further improved, but for the simulations to best

represent reality, additional field data defining the velocity field within 0.4 m of the dipole well would be required.

4.8 Conclusions

The difficulties in modeling a dipole flow system led to using PVPs to map groundwater velocities in the aquifer at an unprecedented level of detail. The field measured velocities were found to be higher proximal to the dipole well than predicted using an homogenous, isotropic aquifer model, and average field-measured *K* estimates. Additional simulations using Visual MODFLOW Pro®, assuming steady-state flow, showed that the measured breakthrough curves could be better described by assuming material proximal to the dipole well that was more permeable than the surrounding aquifer, and less permeable material further away, consistent with the PVP velocity data. A permeability increase of as little as 12% was sufficient to improve the model-experiment BTC match. It was further shown that the BTCs were insensitive to continuous horizontal layering of the aquifer between the dipole screen intervals, partially because the BTCs were minimally affected by changes to the aquifer properties affecting the more distal flowpaths. Under the conditions of these tests, the dipole well BTCs were only sensitive to aquifer properties less than 0.4 meters radial distance from the well.

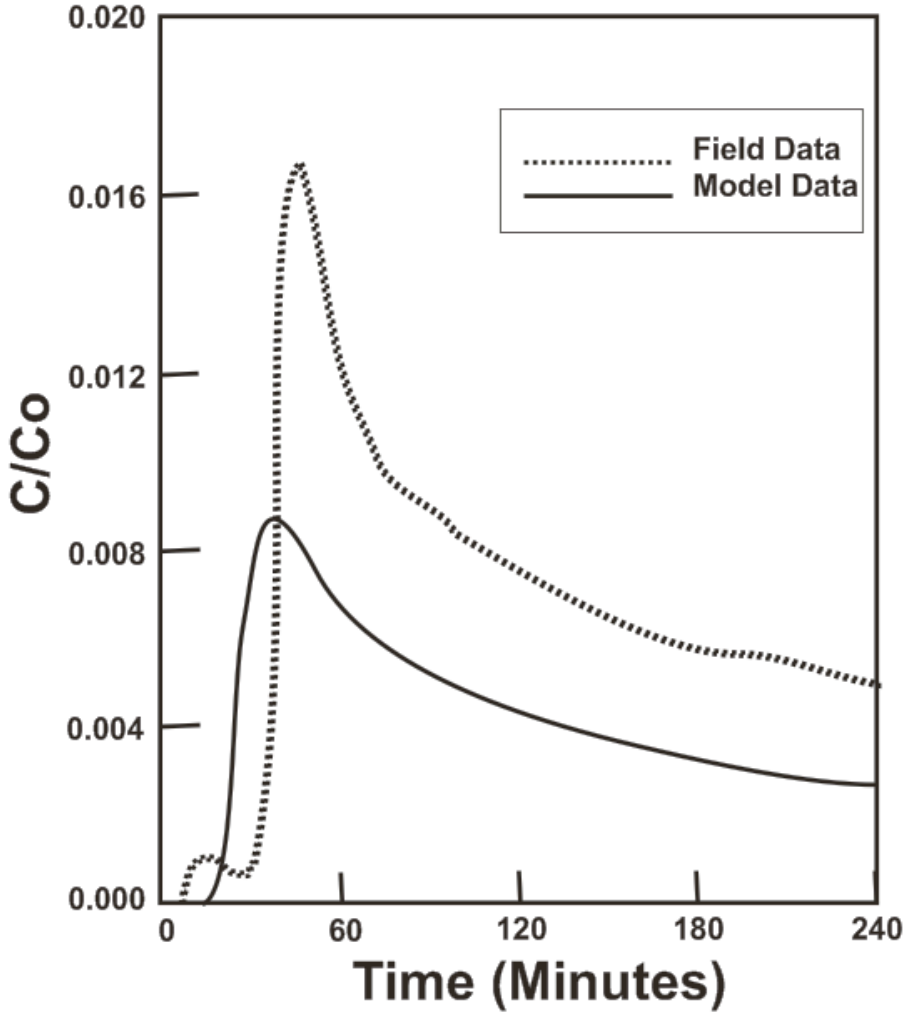

Figure 4.1: Comparison of DFRTT data collected at ~700 mL/min and the model prediction. Adapted from Roos, 2009.

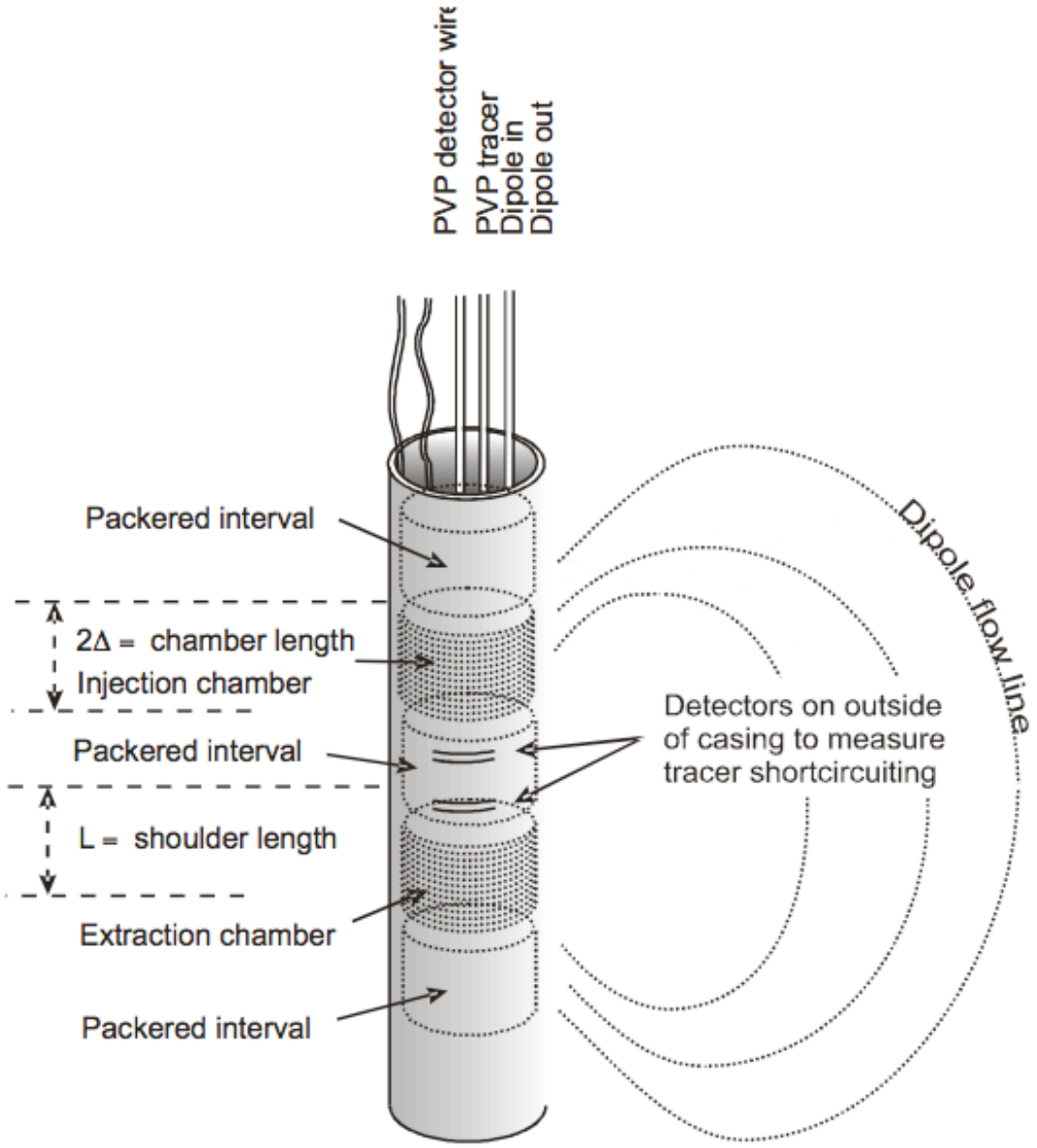

Figure 4.2: Schematic of device to test well skin velocities. PVP Style detectors were placed between the two sections of screen on the dipole well. The detectors and screen between the injection and extraction chamber were sealed and secured with epoxy. The characteristic dimensions 2Δ and L determine the dimensions of the flow system

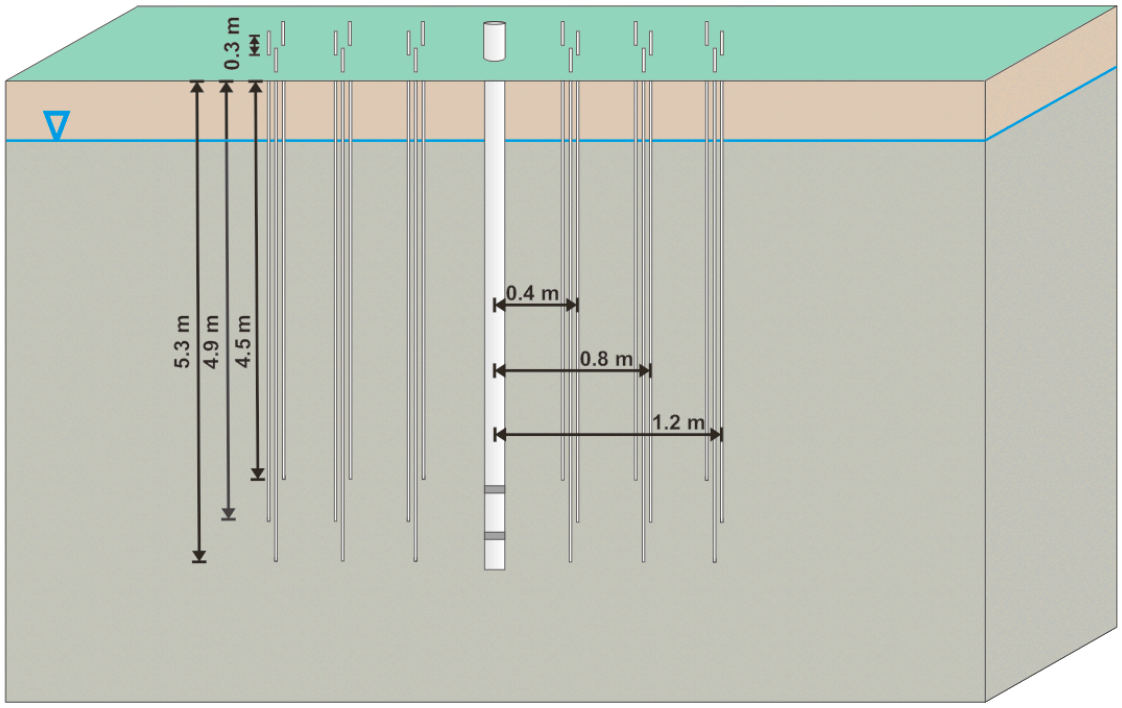

Figure 4.3: Experimental Design depicting orientation of well MW-3 (Center) and the 18 PVPs surrounding it in 3 dimensions.

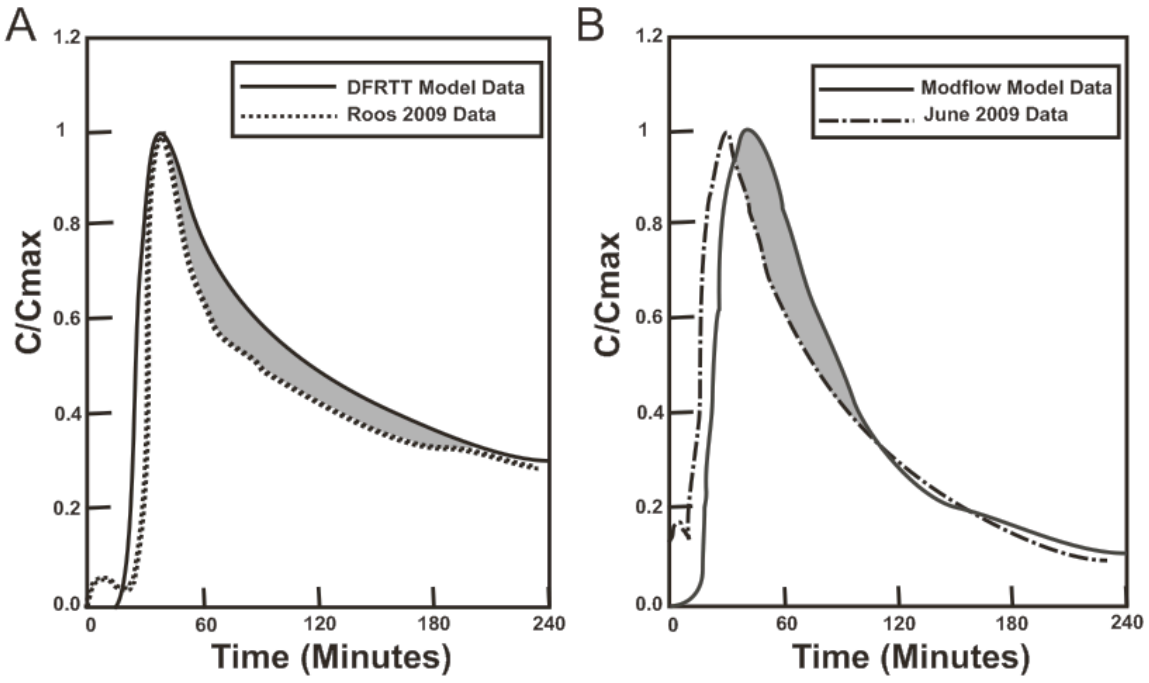

Figure 4.4: Comparison of model and tracer test data. The curves are normalized by the peak concentration to show the differences in the falling limbs. The shaded section shows the deviation from preliminary modeled behavior that led to this work.

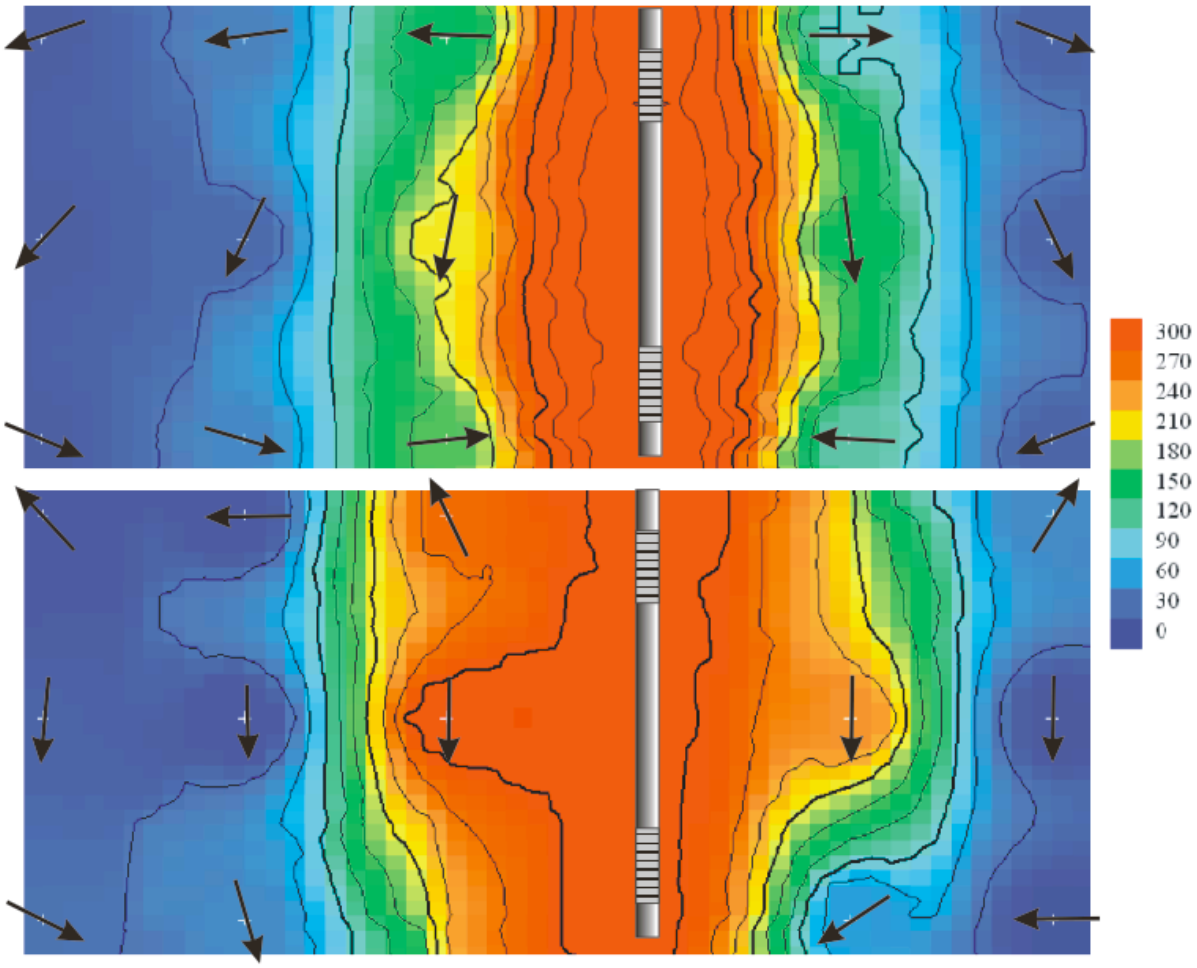

Figure 4.5: Projected cross section of PVP Results (Bottom) as contrasted with the Visual MODFLOW® Model (Top). Velocities are reported in cm/day.

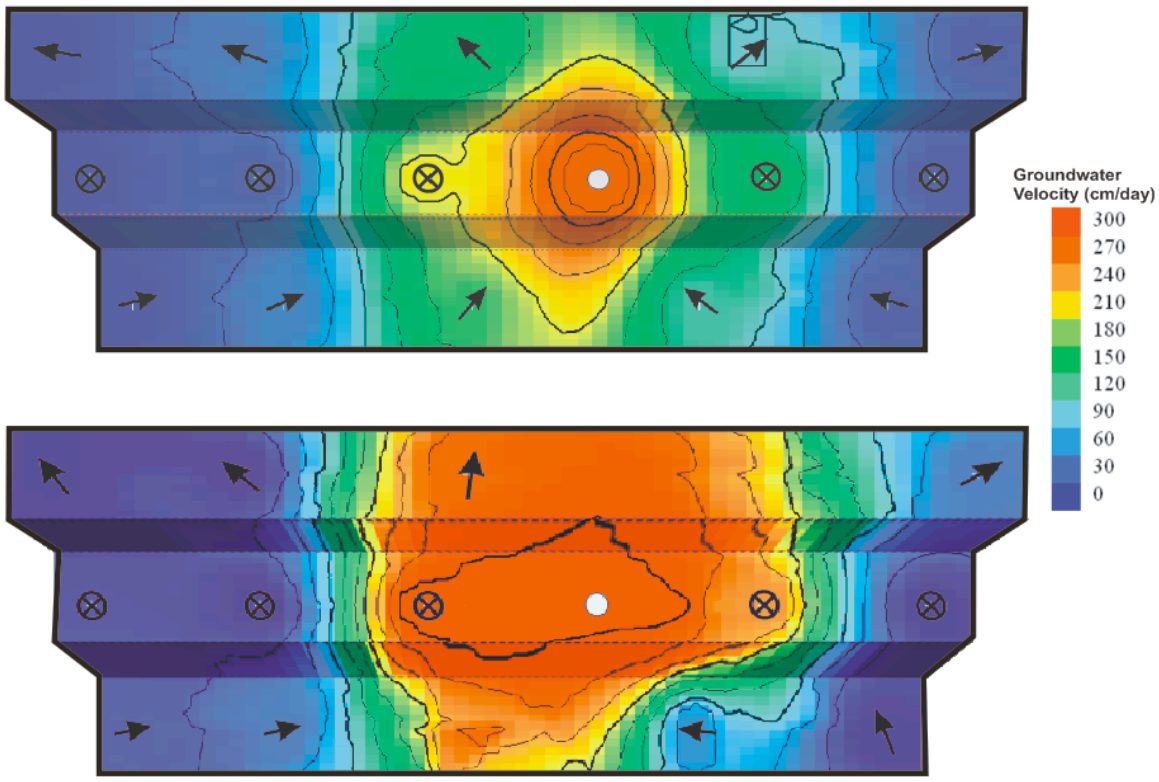

Figure 4.6: Plan View of PVP Results (Bottom) as contrasted with the Visual MODFLOW® Model (Top). North is toward the top of the diagrams. The direction markers indicate the dominant flow direction at each location. Velocities are reported in cm/day. It should be noted that the upper row of PVPs are installed at 4.5m BGS, the middle row is 4.9 m BGS, and the bottom row is 5.3 m BGS.

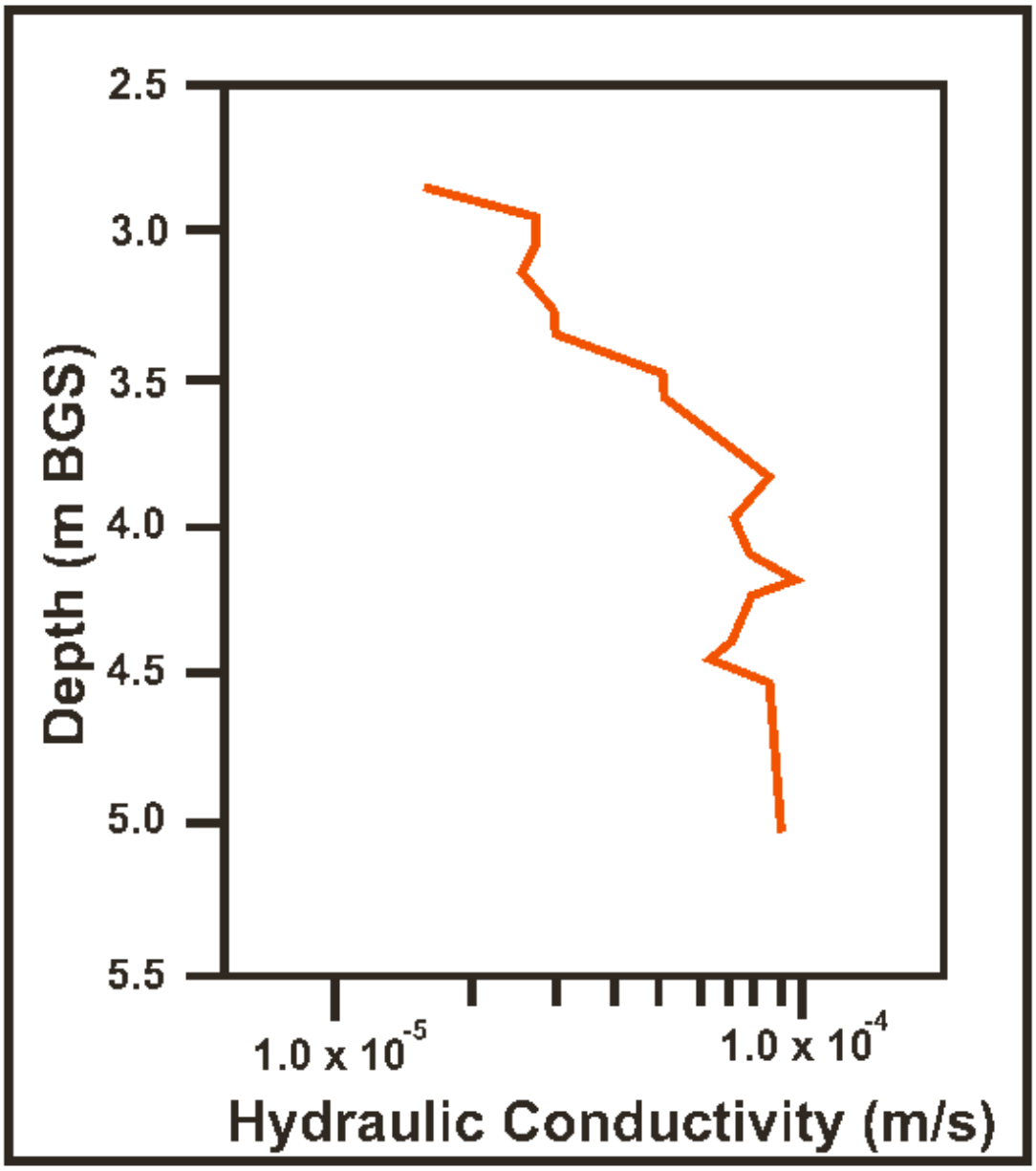

Figure 4.7: Hydraulic conductivity profile of Well MW-3. The lower hydraulic conductivity area near 4.5 m BGS is near the depth of the shallow PVPs.

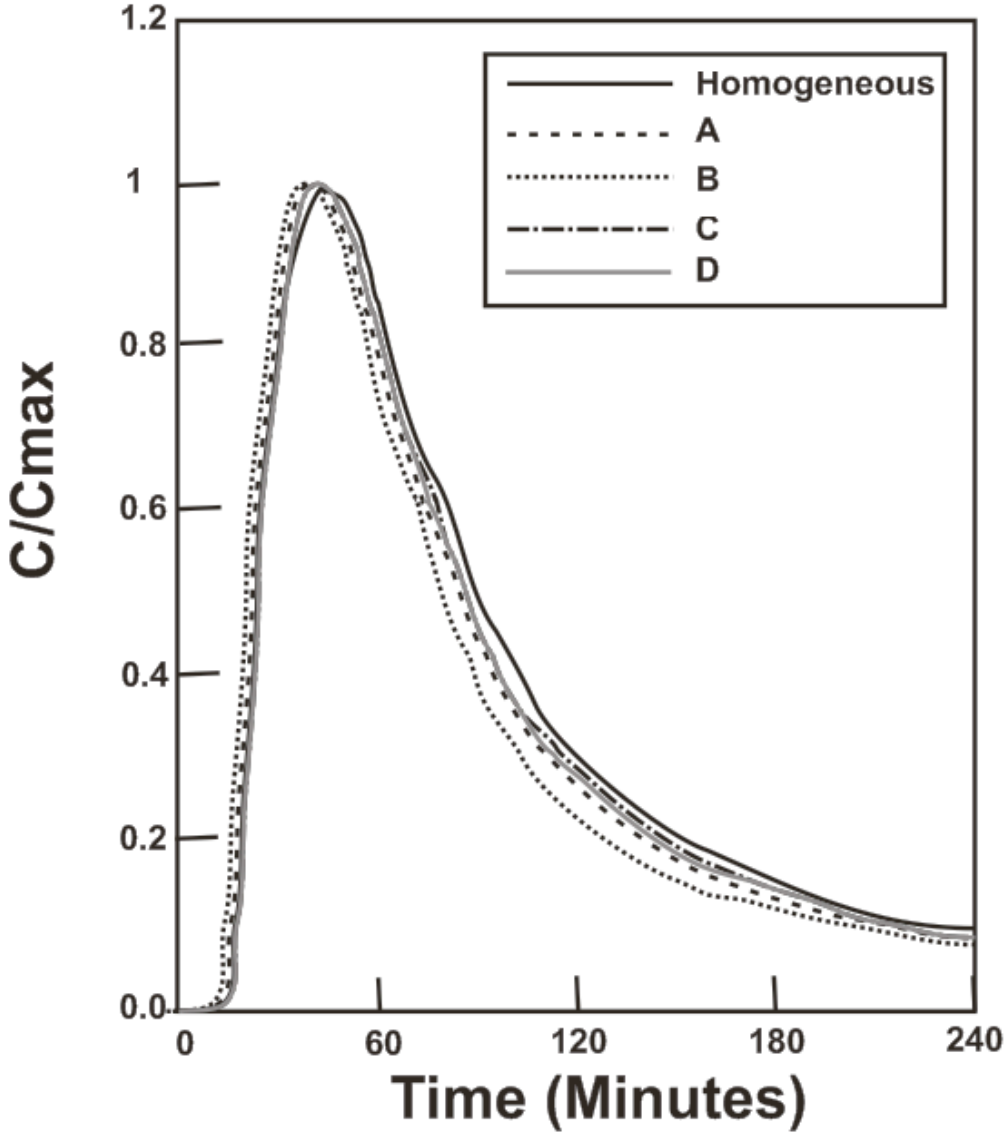

Figure 4.8: Tracer breakthrough curves as estimated using Visual MODFLOW. Curve A simulates a layer of lower hydraulic conductivity (K = 3.87 x 10^{-5} m/s) is placed near the injection portion of the dipole. Curve B simulates a layer of higher hydraulic conductivity (K = 5.8 x 10^{-5} m/s) placed between the screens of the well. Curve C (K = 3.87 x 10^{-5} m/s) simulates tracer breakthrough when an area of lower hydraulic conductivity is placed near the extraction screen. Curve D shows the BTC associated with a small zone of high hydraulic conductivity (K = 8.7 x 10^{-5} m/s) near the well. The results suggest the BTC behavior is insensitive to heterogeneity at distance from the well.

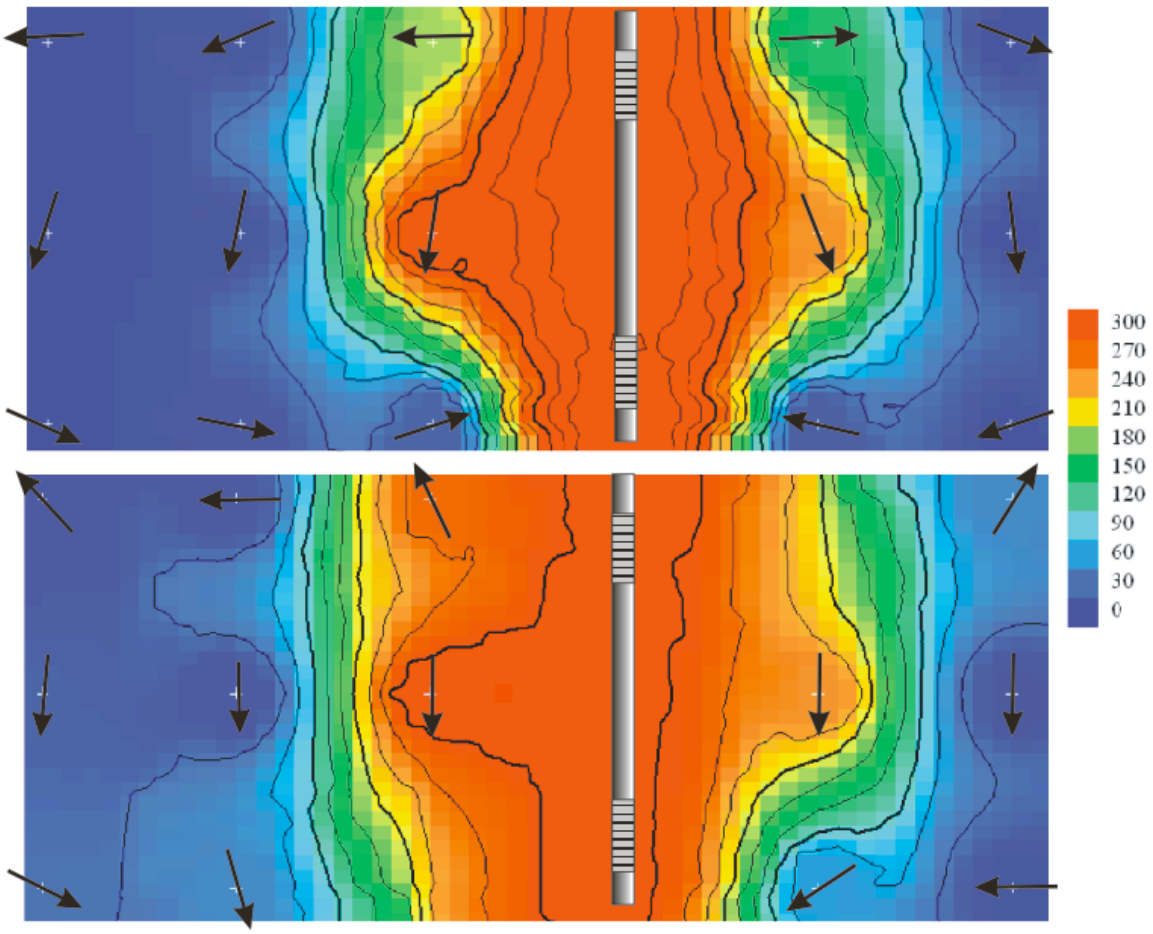

Figure 4.9: Projected cross section of PVP Results (Bottom) as contrasted with the Visual MODFLOW® Model (Top). In this model, a layer of high hydraulic conductivity surrounding the well is simulated. Velocities are reported in cm/day.

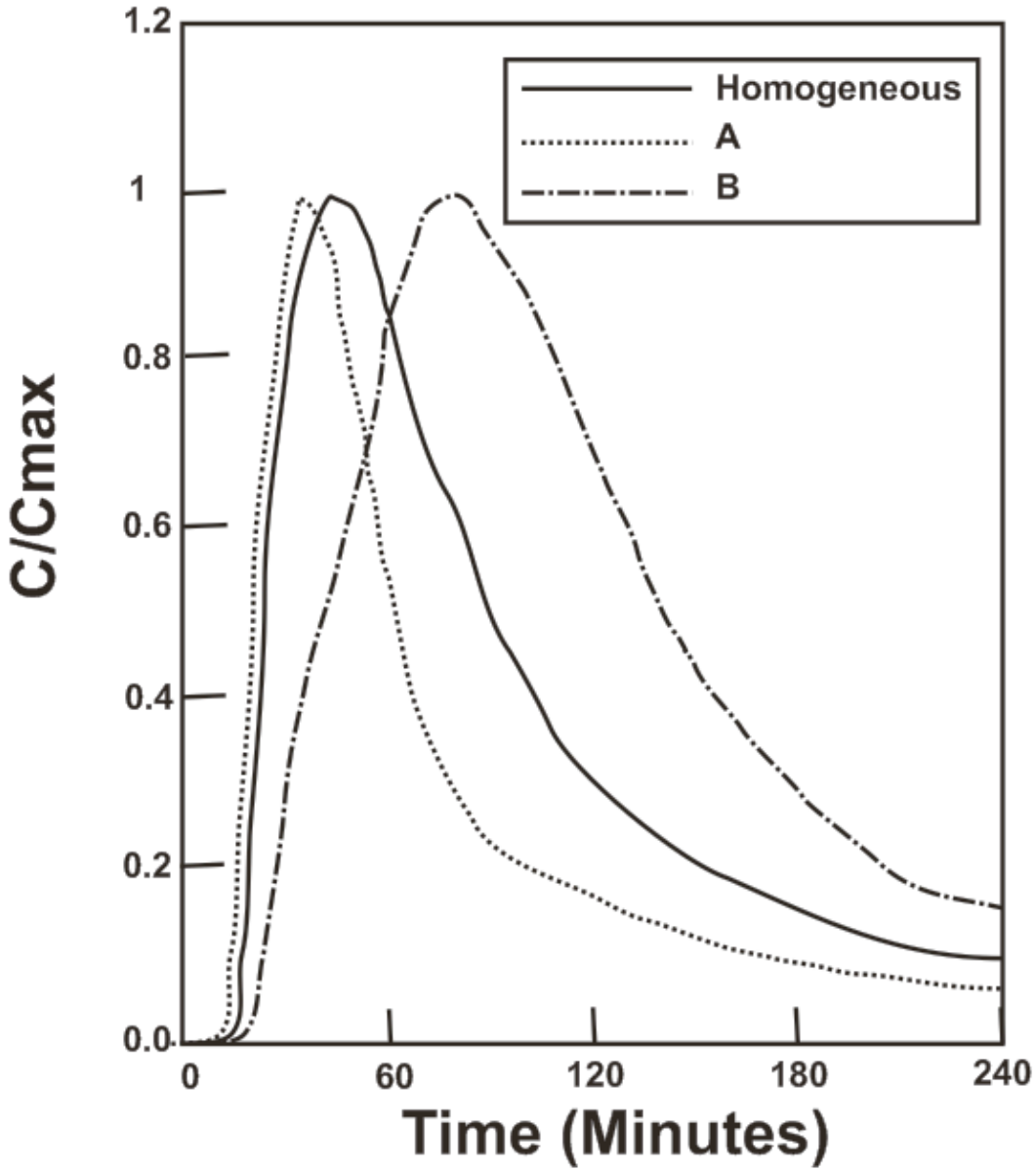

Figure 4.10: Tracer BTCs as estimated by Visual MODFLOW®. Curve A simulates a highly conductive area proximal to the well using a zone of high hydraulic conductivity near the well. Curve B simulates a less conductive zone proximal to the well using a lower hydraulic conductivity zone. These results suggest that tracer BTC behavior is very sensitive to heterogeneity very near the well.

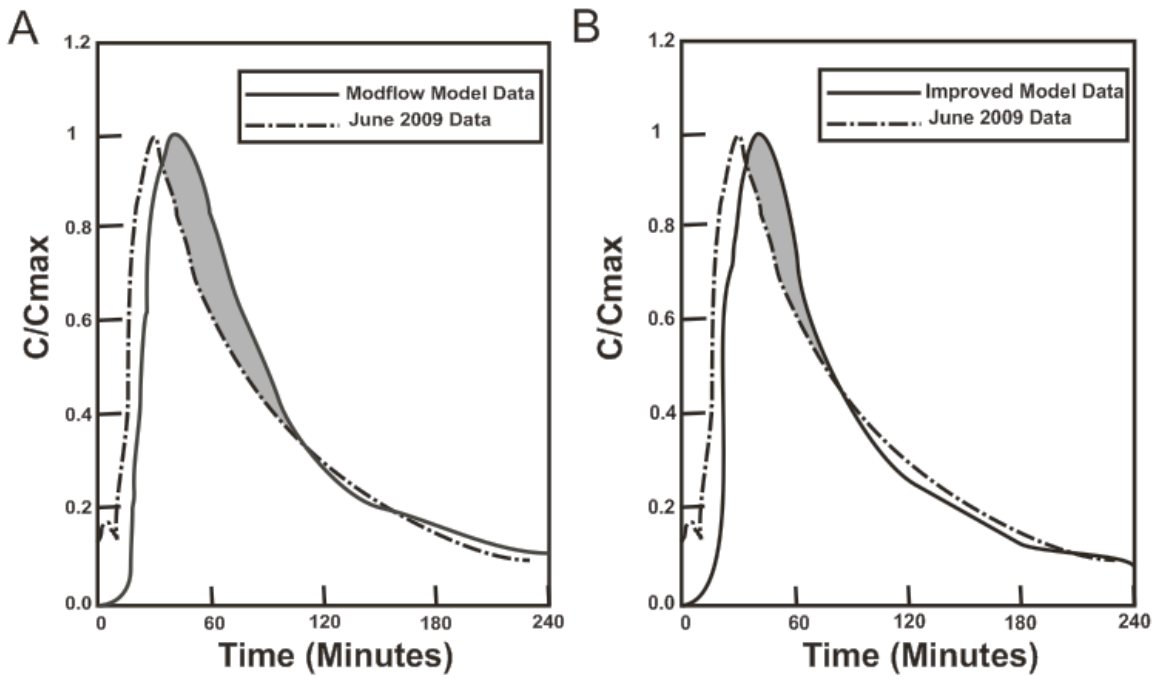

Figure 4.11 Comparison of breakthrough curves for the homogeneous case (A) and the best fitting heterogeneous case (B). The curves are normalized by the peak concentration to show the differences in the falling limbs. The shaded section shows the deviation from modeled behavior.

Chapter 5.

Parameter Optimization Using Velocity Data

5.1 Introduction

Direct velocity measurements are useful for determining contaminant transport pathways and other hydrogeologic information. These measurements are related to the *K* of a formation, but are not subject to the high uncertainty associated with measuring *K* or, in some cases, the hydraulic gradient (Devlin and McElwee, 2007). This independence may prove useful for helping to determine model input parameters for complex hydrogeologic systems such as the flow surrounding a dipole well.

Aquifer parameter estimation and optimization features have been available in commercial groundwater models for several years. Usually, the software optimized the *K* field to provide a best fit for simulated tracer breakthrough data or hydraulic head measurements to measured data. However, there are no commercial or published models capable of performing parameter estimation based on velocity data known to the author at this time. In this work, a simple 2D model is developed to optimize *K* estimates based on direct velocity measurements to demonstrate how velocity data might be used in conjunction with modern numerical models.

5.2 Model Development

The model to be used in this demonstration is based on the heterogeneous 2D general flow equation at steady state (1):

$$\left(\frac{\partial}{\partial x}\left(K_x \frac{\partial h}{\partial x}\right)+\frac{\partial}{\partial y}\left(K_y \frac{\partial h}{\partial y}\right)\right)=0 \quad (1)$$

where K_x and K_y are the hydraulic conductivities in the x and y directions, respectively, and h is the hydraulic head.

The equation can be approximated using finite differences (Equation 2):

$$\frac{\left[K_{i,j}^{i+1,j}\left(\frac{h_{i+1,j}-h_{i,j}}{\Delta x}\right)-K_{i-1,j}^{i,j}\left(\frac{h_{i,j}-h_{i-1,j}}{\Delta x}\right)\right]}{\Delta x}+\frac{\left[K_{i,j}^{i,j+1}\left(\frac{h_{i,j+1}-h_{i,j}}{\Delta y}\right)-K_{i,j-1}^{i,j}\left(\frac{h_{i,j}-h_{i,j-1}}{\Delta y}\right)\right]}{\Delta y}=0 \quad (2)$$

where K is the effective hydraulic conductivity between the nodes referred to by the superscripts and subscripts, h is the hydraulic head at the node referred to by the subscripts, and Δx and Δy are the distances between nodes in the x and y directions. The hydraulic head at the central location is h_{ij}. The subscript i gives the position in the x direction and j denotes its position in the y direction.

The effective hydraulic conductivity between two nodes is calculated from the harmonic mean of the hydraulic conductivities on the nodes of interest (Equation 3).

$$K_{i-1}^{i}=\frac{2K_iK_{i-1}}{K_i+K_{i-1}} \quad (3)$$

Equation 3 is substituted for the effective hydraulic conductivities in equation 2, and it is assumed that Δx and Δy are equal. After these steps, the equation can be solved for the head at each node as seen in Equation 4:

$$h_{i,j} = \frac{h_{i+1,j}\left(\frac{2K_{i,j}K_{i+1,j}}{K_{i,j} + K_{i+1,j}}\right) + h_{i-1,j}\left(\frac{2K_{i,j}K_{i+1,j}}{K_{i,j} + K_{i-1,j}}\right) + h_{i,j+1}\left(\frac{2K_{i,j}K_{i,j+1}}{K_{i,j} + K_{i,j+1}}\right) + h_{i,j-1}\left(\frac{2K_{i,j}K_{i,j-1}}{K_{i,j} + K_{i,j-1}}\right)}{\left(\frac{2K_{i,j}K_{i+1,j}}{K_{i,j} + K_{i+1,j}}\right) + \left(\frac{2K_{i,j}K_{i-1,j}}{K_{i,j} + K_{i-1,j}}\right) + \left(\frac{2K_{i,j}K_{i,j+1}}{K_{i,j} + K_{i,j+1}}\right) + \left(\frac{2K_{i,j}K_{i,j-1}}{K_{i,j} + K_{i,j-1}}\right)} \quad (4)$$

These equations form the basis for estimating the hydraulic head at any point in the model domain. The system to be modeled is a projected cross section of the dipole system discussed previously (Chapter 4). The physical system is actually radial in geometry, but for the purposes of this demonstration the 2D formulation is a reasonable approximation. To represent the injection and extraction nodes in the dipole, a modification is made to equation 4 so the pumping rate (*Q*) can be used instead of fixing head values (equation 5):

$$h_{i,j} = \frac{h_{i+1,j}\left(\frac{2K_{i,j}K_{i+1,j}}{K_{i,j} + K_{i+1,j}}\right) + h_{i-1,j}\left(\frac{2K_{i,j}K_{i+1,j}}{K_{i,j} + K_{i-1,j}}\right) + h_{i,j+1}\left(\frac{2K_{i,j}K_{i,j+1}}{K_{i,j} + K_{i,j+1}}\right) + h_{i,j-1}\left(\frac{2K_{i,j}K_{i,j-1}}{K_{i,j} + K_{i,j-1}}\right)}{Q + \left(\frac{2K_{i,j}K_{i+1,j}}{K_{i,j} + K_{i+1,j}}\right) + \left(\frac{2K_{i,j}K_{i-1,j}}{K_{i,j} + K_{i-1,j}}\right) + \left(\frac{2K_{i,j}K_{i,j+1}}{K_{i,j} + K_{i,j+1}}\right) + \left(\frac{2K_{i,j}K_{i,j-1}}{K_{i,j} + K_{i,j-1}}\right)} \quad (5)$$

The equations were used in a spreadsheet model with constant-head boundaries at the left and right sides of the domain and no-flow boundaries at the top and bottom. Following the definition of the boundary conditions, equation 4 was copied into each cell and equation 5 was placed where the injection and extraction points of the dipole were located. The model calculated hydraulic heads iteratively, based on the neighboring hydraulic head values, hydraulic conductivity, and the distances between the nodes.

The hydraulic head values were used to determine groundwater velocities in the horizontal and vertical directions using Darcy's Law. These vector values were used to determine the total velocities at each node, which were compared to the measured velocities.

The residual sum of squares (RSS) between the measured and modeled velocities were used to optimize the model. This was accomplished using the solver tool in Microsoft Excel® to vary the hydraulic conductivities of selected zones within the domain to minimize the RSS.

5.3 Results

The model was designed with the hydraulic conductivity at each node specified. While this flexibility could result in a perfectly optimized velocity field, the results would not necessarily be geologically meaningful. Therefore, zones of varying *K* were inferred in the domain on the basis of the PVP velocity measurements, and the results of Chapter 4 (Figure 5.1). This analysis considered 3 hydraulic conductivity zones where groups of PVPs had significantly different speeds (Figures 5.1 and 5.2). The initial guesses for the hydraulic conductivities were selected to give reasonable fits to the velocity data (Table 5.1). Once the preliminary velocity comparisons were satisfactory, the solver tool was used to optimize the hydraulic conductivities to obtain a best fit.

Before optimization, many of the velocities modeled for large distances from the well were higher than the measured velocities. These discrepancies are seen in the lower-left region of Figure 5.3A. Also, the model velocities near the well (with higher magnitudes) were slower than measured (Figure 5.3A). The solver-optimized solution provided an improved match between the experimental and modeled velocities compared to a simulation assuming an homogeneous aquifer (Figure 5.3). Apart from one outlying point where a good fit could not be

obtained, the measurements generally fell near the line of perfect agreement between modeled velocity and measured velocity. The optimized velocity solution resulted in a zone with 35% higher hydraulic conductivity near the well than the background estimates. This result was similar in magnitude to the 12% conductivity difference seen in the best breakthrough-curve match seen in Chapter 4, and demonstrated the sensitivity of the flow system to heterogeneity close to the well.

5.4 Conclusions

Direct velocity measurements can be used as an optimization tool for groundwater modeling. However, no off-the-shelf tools yet exist to use this type of data for optimization. In this work, a simple model was used to optimize hydraulic conductivity estimates using velocity. The results show marked improvement in the match between modeled and experimentally determined velocity estimates, and demonstrated the utility of the technique. The optimized velocity model used a hydraulic conductivity near the well that was 35% higher than the background value. This small change further demonstrated the sensitivity of the flow system to the area proximal to the well and was similar in magnitude to the best match breakthrough curve solution seen in Chapter 4. In the future, this model could be adapted to three-dimensions, and similar techniques could be adapted to commercial modeling software.

Table 5.1: Hydraulic conductivity values used in velocity optimization.

Zone	Hydraulic Conductivity Initial Trial (m/s)	Hydraulic conductivity Trial 2 (m/s)	Optimized Hydraulic conductivity (m/s)
Measured Velocities Faster than Modeled Velocities (Yellow Zone)	1.74×10^{-4}	1.39×10^{-4}	1.38×10^{-4}
Measured Velocities Slower than Modeled Velocities (Blue Zone)	5.79×10^{-6}	5.79×10^{-6}	4.63×10^{-6}
Background (White Zone)	1.16×10^{-4}	1.04×10^{-4}	8.98×10^{-5}

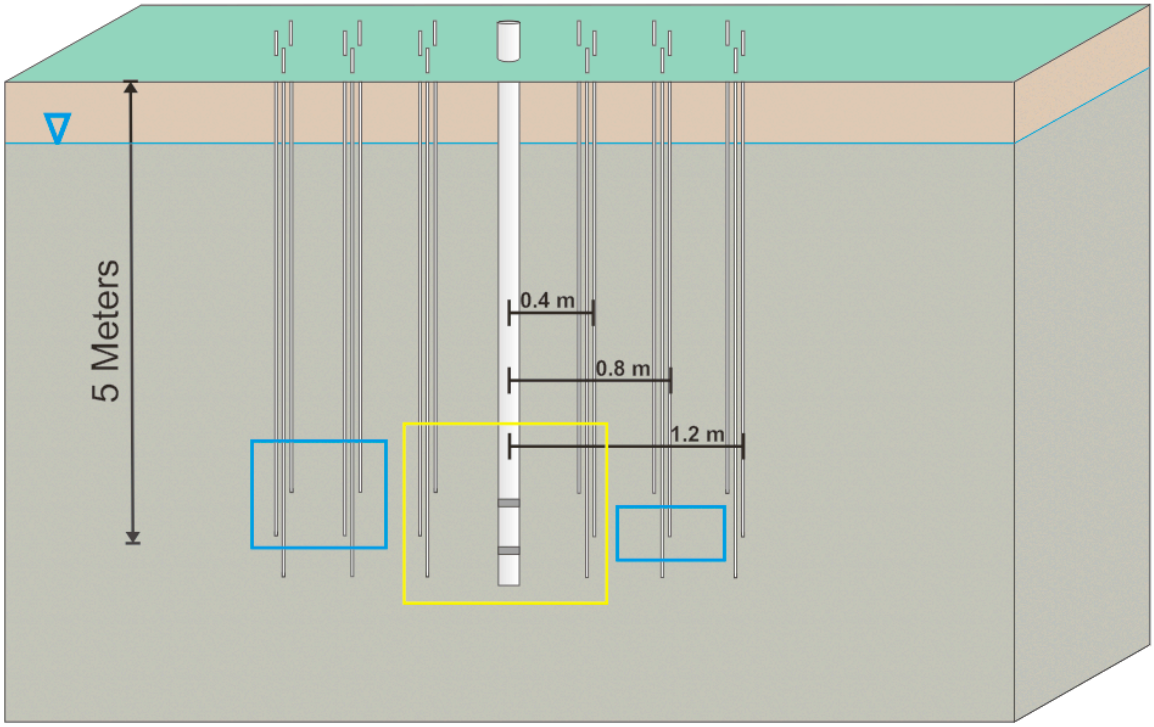

Figure 5.1: The location of PVPs in cross section. The PVP measured velocities are projected into the same plane in the model. The yellow region corresponds with the PVP measured velocities that were higher than expected. The blue region corresponds with PVP measured velocities that were lower than expected.

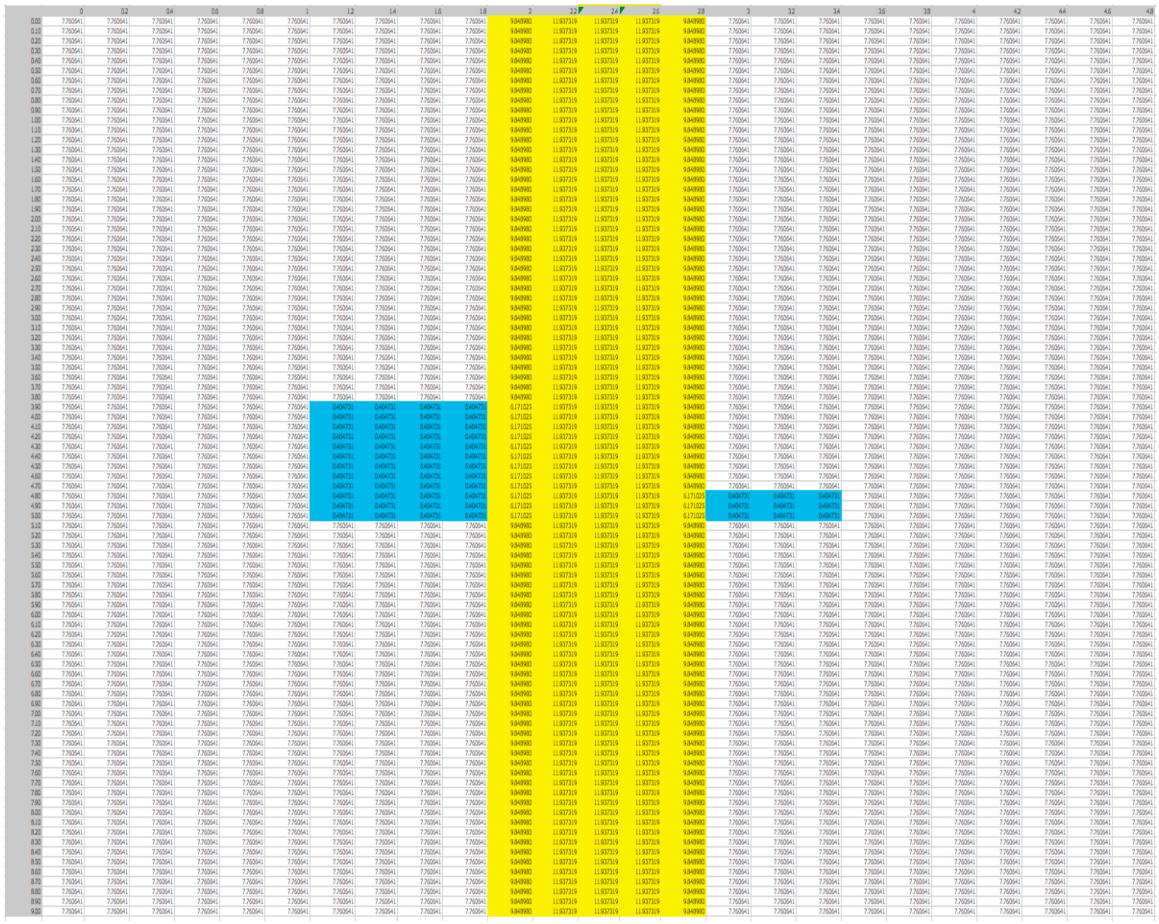

Figure 5.2: The hydraulic conductivity field of the model. The yellow region corresponds with the PVP measured velocities that were higher than expected. The blue region corresponds with PVP measured velocities that were lower than expected.

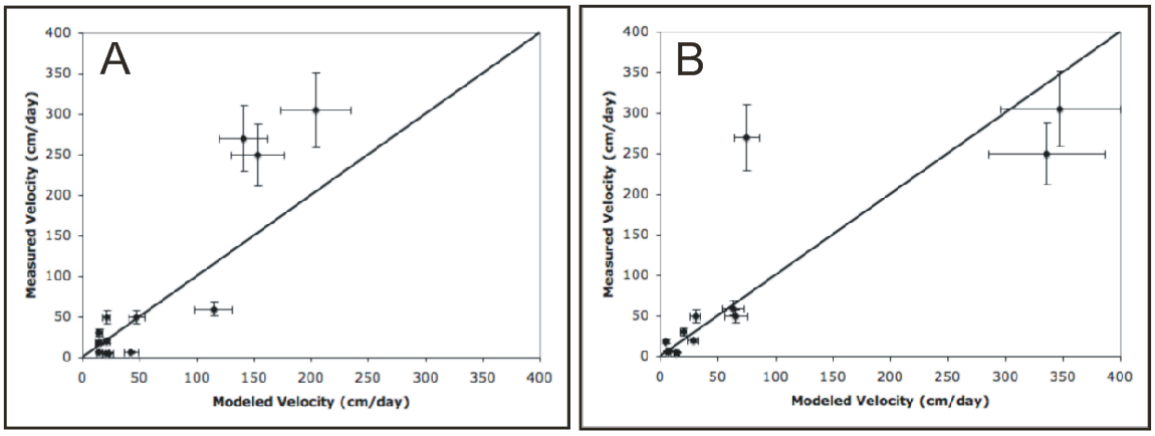

Figure 5.3: Measured and modeled velocity comparison for the homogeneous (A) and optimized (B) velocity models. The line represents the best case where both velocities are equal.

Chapter 6: Conclusions and Recommendations

6.1 Conclusions

The objectives of this thesis were: Design, construct, and test a simple, inexpensive, and leak resistant apparatus suitable for creating a controlled flow system in porous media at the benchtop scale; design, construct, laboratory test, and field-test a prototype PVP capable of measuring horizontal and vertical flow; design, construct, and field-test a device capable of measuring groundwater velocity in the well skin of an operating dipole well; and characterize the flow system around a dipole well to assist in the simulation of tracer movement in the aquifer during a Dipole Flow and Reactive Tracer Test with a numerical model.

The need for an inexpensive flow-through tank design resulted in the design and construction of the Nested Storage Tank system, NeST. This system was designed as an easy-to-construct apparatus for laboratory testing where a well-controlled flow system was required. The flow was uniform in the tank ~10 cm and beyond from the upgradient boundary, which was non-uniform because of the irrigation fittings. There were no observable boundary effects in the center of the porous medium where most tests were conducted. Furthermore, the velocity was predictable and several different velocity estimates agreed within 25%. Much of the uncertainty in velocity was attributable to the porosity, which was difficult to measure precisely. The NeST is suitable for many applications where a flow-through tank is desired including teaching and research.

The PVP presented in this work is a novel design, which is smaller than the previously available PVPs and constructed using a different technique. The

PVP is capable of measuring horizontal and vertical flow with an average uncertainty in magnitude of 15% and an average uncertainty in direction of ± 8°. These results agree well with previous PVP designs in sandy material, but showed a small negative bias (Labaky *et al.,* 2007). The velocities determined using the PVP was also compared to velocities calculated for the NeST using flow and tracer tests. The complete suite of velocities agreed to within 25% in velocity magnitude, despite operating on different principles and scales. These results suggest the PVP can successfully characterize flow in a 3-dimensional flow system in sandy material.

After testing the Point Velocity Probe in the laboratory using the NeST, an array of probes was deployed surrounding an operating dipole well in the field. The PVP results indicate velocities were faster near the well than predicted by a model. Furthermore, the areal extent of the test was smaller than an homogeneous-aquifer model predicted. These results helped explain some of the differences observed in breakthrough curve behavior in a Visual MODFLOW Pro® model using the MT3DMS transport engine (Zheng and Wang, 1999). The model results show that many different types of distal heterogeneity can result in similar breakthrough curve behavior. However, the area within 0.4 m of the well is critical to the shape of the BTC.

A device to determine velocity in the well skin of an operating dipole well was also designed and used. This device showed that velocity in the zone immediately next to the outside of the casing was very fast. In the case of the filter packed well, the average velocity was ~8500 cm/day for a pumping rate of

300 mL/min. The results at the non-filter packed well and at higher flow rates were difficult to interpret because the resolution of the datalogger was insufficient to discern arrival times of the tracer at the detectors. Despite this difficulty, the velocity appears to be much faster than in the non-filter packed well and suggests a near-instantaneous transmittal of tracer from the injection screen to the extraction screen.

Finally, a simple model was developed to optimize hydraulic conductivity values using measured velocities. This model demonstrated that two-dimensional model velocity estimates could be improved using the technique. A 2D model is limited, but it was beyond the scope of this work to develop a three-dimensional model with a connected nonlinear optimizer..

6.2 Recommendations

This research focused on the development of a small PVP capable of measuring flow in 3-dimensions. This type of data is desirable for characterizing complex flow found in remediation systems. Development of the PVP should be furthered to provide high-quality velocity data for many projects. The manufacturing process currently limits the speed of PVP design evolution. Automating the construction of PVPs with a rapid prototyping machine could overcome this limitation, and should be pursued.

Another area that requires further investigation is the affect of PVP size on velocity. Preliminary results presented in Appendix D indicate a possible size

bias, but this is not supported theoretically. Therefore, a systematic investigation of this effect is recommended.

In the case of the Dipole Flow and Reactive Tracer Test, the area very close to the well appears to be crucial to the breakthrough curve results. The PVPs were placed at distances of 0.4 m and greater from the well. PVPs placed even closer to the well may be able to provide more information inside this critical zone. The model results suggest that heterogeneity at greater distances has less affect on the BTC behavior, but a heterogeneous model may be necessary to accurately estimate aquifer parameters using the DFRTT. Further work could be done to characterize the velocity in the well skin of a DFRTT by increasing datalogger resolution, or increasing the separation of the detectors.

The utility of direct velocity measurements in modeling was demonstrated in Chapter 5. However, the work was limited to the 2D case. Developing a 2D radial flow model, or a 3D model would make this optimization more valuable. Adding parameter estimation and optimization using velocity data to an off-the-shelf model would enhance the utility of direct velocity measurements and allow wider access to the optimization tools.

References:

Ballard, S. **1996**. The In Situ Permeable Flow Sensor: ground-water flow velocity meter. *Ground Water* vol. 34, no. 2: 231-240.

Barns, G.L., R.D. Wilson, and S.F. Thornton. **2010**. Assessing of the effect of physical heterogeneity on single well tracer tests using imaging experiments. *Proceedings, 7th International Groundwater Quality Conference*. Zurich, Switzerland, June 13-18, 2010.

Barrash, W., T. Clemo, J.J. Fox, and T.C. Johnson. **2006**. Field, laboratory, and Modeling investigation of the skin effect at wells with slotted casing, Boise Hydrogeophysical Research Site. *Journal of Hydrology* vol. 326: 181-198.

Barth, G.R., Hill, M.C., Illanasekare, T.H., and Rajaram, H. **2001**. Predictive Modeling of Flow and Transport in a Two-dimensional Intermediate-scale, Heterogeneous Porous Medium. *Water Resources Research* vol. 37, no. 10: 2503-2512.

Berg, S.J., and R.W. Gillham. **2010**. Studies of Water Velocity in the Capillary Fringe: The Point Velocity Probe. *Ground Water* vol. 48, no. 1: 59-67.

Bi, E., Devlin, J.F., and Huang, B. **2009**. Effects of Mixing Granular Iron with Sand on the Kinetics of Trichloroethylene Reduction. *Ground Water Monitoring and Remediation* vol. 29, no. 2: 56-62.

Brewster, M.L., Annan, A.P., Greenhouse, J.P., Kueper, B.H., Olhoeft, G.R., Redman, J.D., and Sander, K.A. **1995**. Observed migration of a controlled DNAPL release by geophysical methods. *Ground Water* vol. 33, no. 6: 977-987.

Butler, James J. Jr. **1997**. The design, performance, and analysis of slug tests. CRC Press, Lewis Publishers.

Butler, James J. Jr. **2005**. Hydrogeological methods for estimation of spatial variations in hydraulic conductivity. *Hydrogeophysics*, Y. Rubin and S.S. Hubbard (eds.). Springer: 23-58.

Close, M., Bright, J., Wang, F., Pang, L. and Manning, M. **2008**. Key Features of Artificial Aquifers for Use in Modeling Contaminant Transport. *Ground Water* vol. 46, no. 6: 814-828.

Danquigny, C., Ackerer, P., and Carlier, J.P. **2004**. Laboratory Tracer Tests on Three-dimensional Reconstructed Heterogeneous Porous Media. *Journal of Hydrology* vol. 294, no. 1-3:196-212.

Darcy, H. **1856**. *Les Fontaines Publiques de la Ville de Dijon*, Dalmont, Paris.

Devlin, J.F. 1994. A simple and powerful method of parameter-estimation using simplex optimization. *Ground Water* vol. 32, no. 2: 323-327.

Devlin, J.F. and C.M. McElwee. **2007**. Effects of measurement error on horizontal hydraulic gradient estimates in an alluvial aquifer. *Ground Water* vol. 45, no. 1: 62-73

Devlin, J.F., G. Tsoflias, M. McGlashan, and P. Schillig. **2009**. An inexpensive multilevel array of sensors for direct ground water velocity measurement. *Ground Water Monitoring & Remediation* vol. 29, no. 2: 73-77.

Di Biase, S.M. **1999**. An experimental method in groundwater flow measurement: the development of a groundwater velocity probe. B. Sc. thesis, Department of Earth Sciences, University of Waterloo, Waterloo, Ontario, Canada.

Drost, W., D. Klotz, A. Koch, H. Moser, F. Neumaier, and W. Rauert. **1968**. Point dilution methods of investigating ground water flow by means of radioisotopes. *Water Resources Research* vol. 4, no. 1: 125-145, doi:10.129/WR004i001p00125.

Faust, C. R., and J. W. Mercer. **1984**. Evaluation of Slug Tests in Wells Containing a Finite-Thickness Skin. *Water Resources Research* vol. 20, no. 4: 504-506.

Fetter, C.W. **2001**. Applied Hydrogeology. Prentice Hall, Inc.

Gavaskar, A.R. **1999**. Design and construction techniques for permeable reactive barriers. *Journal of Hazardous Materials* vol. 68, no. 1-2: 41-71

Gierczak, R.F.D., J.F. Devlin, and D.L. Rudolph. **2006**. Combined use of field and laboratory testing to predict preferred flow paths in an heterogeneous aquifer. *Journal of Contaminant Hydrology* vol. 82: 75-98.

Guilbeault, M.A., B.L. Parker, and J.A. Cherry. **2005**. Mass and Flux Distributions from DNAPL Zones in Sandy Aquifers. *Ground Water* vol. 43, no. 1: 70-86.

Hess, K.M. J.A. Davis, D.B. Kent, and J.A. Coston. **2008**. Multispecies reactive tracer test in an aquifer with spatially variable chemical conditions, Cape Cod, Massachusetts: Dispersive transport of bromide and nickel. *Water Resources Research* vol. 38, no. 8: 10.1029/2001WR000945.

Hyder, Z., and J. J. Butler, Jr. **1995**. Slug Tests in Unconfined Formations: An Assessment of the Bouwer and Rice Technique. *Ground Water* vol. 33, No. 1: 16-22.

Johnson, R.L. and M.A. Simon. **2007**. Evaluation of Groundwater Flow Patterns around a dual-screened groundwater circulation well. *Journal of Contaminant hydrology* vol. 93: 188-202.

Kabala, Z.J. **1993**. The dipole flow test: a new single-borehole test for aquifer characterization. *Water Resources Research*, vol. 29, no.1: 99-107.

Kearl, P.M. **1997**. Observations of particle movement in a monitoring well using the colloidal borescope. *Journal of Hydrology* vol. 200: 323-344.

Kerfoot, W.B. and V.A. Massard. **1985**. Monitoring well screen influences on direct flowmeter measurements. *Ground Water Monitoring Review* vol. 5, no. 4: 74-77, doi:10.1111/j.1745-6592.1985.tb00942.x.

Knox, R.C., D.A. Sabatini, J.H. Harwell, R.E. Brown, C.C. West, F. Blaha, C. Griffin. **1997**. Surfactant Remediation Field Demonstration Using a Vertical Circulation Well. *Ground Water* vol. 35, issue 6: 948-953

Kobus, H., B. Barczewski, and H.P. Koschitzky (Eds.). **1996**. Groundwater and Subsurface Remediation. Verlag, Berlin, Heidelberg, Springer.

Labaky, W. **2004**. Theory and testing of a device for measuring point-scale groundwater velocities. Ph.D. thesis, Department of Earth Sciences, University of Waterloo, Waterloo, Ontario, Canada.

Labaky, W., Devlin, J.F., and Gillham, R.W. **2007.** Probe for Measuring Groundwater Velocity at the Centimeter Scale. *Environmental Science and Technology* vol. 41, no. 24: 8453-8458.

Labaky, W. J.F. Devlin, and R.W. Gillham. **2009**. Field comparison of the point velocity probe with other groundwater velocity measurement methods. *Water Resources Research* vol. 45, W00D30, doi:10.1029/2008WR007066

Lee, E.S., Woo, N.C., Schwartz, F.W. Lee B.S., Woo, M.H. Kim, J.H., Kim, H.K. **2008**. Characterization of Controlled-release KMnO4 (CRP) Barrier System for Groundwater Remediation: A Pilot-scale Flow-tank Study. *Chemosphere* vol. 71, no. 5: 902-910.

MacFarlane, D.S., Cherry, J.A., Gillham, R.W., and Sudicky, E.A. **1983**. Migration of contaminants in groundwater at a landfill: A case study: 1. Groundwater flow and plume delineation. *Journal of Hydrology*, vol. 63 no. 1-2: 1-29.

Moench, A.F., and P.A. Hsieh. **1985**. Comment on "Evaluation of Slug Tests in Wells Containing a Finite-Thickness Skin" by C. R. Faust and J. W. Mercer. *Water Resources Research*. vol. 21, no. 9: 1459-1461.

Momii, K., K. Jimmo, and F. Hirano. **1993**. Laboratory studies on a new laser Doppler-velocimeter system for horizontal groundwater velocity measurements in a borehole. *Water Resources Research* vol. 29, no. 2: 283-291, doi:10.1029/92WR01958.

Morkin, M., J.F. Devlin, J.F. Barker, and B.J. Butler. **2000**. In situ sequential treatment of a mixed contaminant plume. *Journal of Contaminant Hydrology* vol. 45: 283-302.

Niemann, W.L. and C.W. Rovey. **2009**. A systematic field-based testing program of hydraulic conductivity and dispersivity over a range in scale. *Hydrogeology Journal* vol. 17, no. 2: 307-320.

Novakowski, K.S. **1989**. A composite analytical model for analysis of pumping tests affected by well bore storage and finite thickness skin. *Water Resources Research* vol. 25, no. 9: 1937-1946.

Nwankwor, G.I., Cherry, J.A., and Gillham, R.W. **1984**. A comparative study of specific yield determinations for a shallow sand aquifer. *Ground Water*, vol. 22, no. 6: 764-772.

Ogata, A., and Banks, R.B. **1961**. A solution of the differential equation of longitudinal dispersion in porous media. U.S. Geological Survey, *Professional Paper No. 411-A*.

Patterson, B.M., Annable, M.D., Bekele, E.B., Furness, A.J. **2010**. On-line groundwater velocity probe: laboratory testing and field evaluation. *Journal of Contaminant Hydrology*, vol. 117: 109-118.

Phillip, R.D., and G.R. Walter. **1992.** Prediction of Flow and Hydraulic Head Fields for Vertical Circulation Wells. *Ground Water* vol. 30, issue 5: 765-773.

Pitrak, M., S. Mares, and M. Kobr. **2007**. A simple borehole dilution technique in measuring horizontal ground water flow. *Ground Water* vol. 45, no. 1: 89-92.

Ramey, H.J., R.G. Agarwal. **1972**. Annulus Unloading Rates as Influenced by Wellbore Storage and Skin Effect. *Society of Petroleum Engineers Journal*. vol. 12, no. 5: 453-462.

Reiha, B. **2006**. A Numerical Interpretation Model for the Dipole Flow and Reactive Tracer Test. M. Sc. thesis, Department of Earth Sciences, University of Waterloo, Waterloo, Ontario, Canada.

Roos, G.N. **2009**. Development of the Dipole Flow and Reactive Tracer Test for Aquifer Parameter Estimation. M. Sc. thesis, Department of Earth Sciences, University of Waterloo, Waterloo, Ontario, Canada.

Rovey, C.W., and D.S. Cherkauer. **1995**. Scale Dependency of Hydraulic Conductivity Measurements. *Ground Water* vol. 33, no. 5: 769-780.

Sabatini, D.A., Knox, R.C., J.H. Harwell, T. Soerens, L. Chen, R.E. Brown, C.C. West. **1997**. Design of a Surfactant Remediation Field Demonstration Based on Laboratory and Modeling Studies. *Ground Water* vol. 35, issue 6: 948-953

Schillig, P.C., J.F. Devlin, J.A. Roberts, G.P. Tsoflias, and M.A. McGlashan. **2010**. Transient Heterogeneity in an Aquifer Undergoing Bioremediation of Hydrocarbons. *Ground Water*. Doi: 10.111/j.1745-6584.2010.00682.x

Schillig, P.C. **2010**. VelProbePE: An Automated Spreadsheet Program for Interpreting Point Velocity Probe Breakthrough Curves. In Preparation.

Schulze-Makuch, D., D.A. Carlson, D.S. Cherkauer, and P. Malik. **1999.** Scale dependency of hydraulic conductivity in heterogeneous media. *Ground Water* vol. 37, no. 6: 904-919.

Silliman, S.E., Zheng, L., and Conwell, P. **1998**. The Use of Laboratory Experiments for the Study of Conservative Solute Transport in Heterogeneous Porous Media. *Hydrogeology Journal* vol. 6: no. 1:166-177.

Simpson, M.J., Clement, T.P., and Gallop, T.A. **2003**. Laboratory and Numerical Investigation of Flow and Transport Near a Seepage-Face Boundary. *Ground Water* vol. 41, no. 5: 690-700.

Sternberg, S.P.K., Cushman, J.H., and Greenkorn, R.A. **1996**. Laboratory Observation of Non-local Dispersion. *Transport in Porous Media* vol. 23: 135-151.

Su, G.W. B.M. Freifeld, C.M. Oldenburg, P.D. Jordan, and P.F. Daley. **2006**. Interpreting velocities from heat-based flow sensors by numerical simulation. *Ground Water* 44, no. 3: 386-393.

Sudicky, E.A. **1986**. A natural gradient experiment on solute transport in a sand aquifer: Spatial variability of hydraulic conductivity and its role in the

dispersion process. *Water Resources Research* vol. 22, no. 13: 2069-2082.

Thomson, N.R., Reiha, B., McKnight, D., Smalley, A.L., and Banwart, S.A. **2005**. An overview of the dipole flow in situ reactor. *In* Proceedings, 33rd Annual Conference of the Canadian Society for Civil Engineering. Toronto, Ontario. June 2-4, 2005.

Tomlinson, D.W., Thomson, N.R., Johnson, R.L., and Redman, J.D. **2003**. Air distribution in the Borden aquifer during I n situ air sparging. *Journal of Contaminant Hydrology* vol. 67, no. 1-4: 113-132.

U.S. EPA. **1999**. "Roy F. Weston, Inc. and IEG Technologies Corporation Unterdruck-Verdampfer-Brunnen (UVB) Technology." EPA/540/R-95/500. March.

U.S. EPA. **2000**. "Technology Evaluation Report for the NoVOCS™ Technology." EPA/540/R-00/502a.

Watson, S.J., Barry, D.A., Schotting, R.J., and Hassanizadeh, S.M. **2002**. On the Validity of Darcy's Law for Stable High-concentration Displacements in Granular Porous Media. *Transport in Porous Media* vol. 47, no. 2: 149-167.

Woodbury, A.D., and Sudicky, E.A. **1991**. The geostatistical characteristics of the Borden aquifer. *Water Resources Research* vol. 27, no. 4: 533-546.

Zheng, C., and P.P. Wang. **1999**. MT3DMS, A Modular Three-Dimensional Multispecies Transport Model for Simulation of Advection, Dispersion, and Chemical Reactions of Contaminants in Groundwater Systems. Documentation and User Guide. Contract Report SERDP-99-1, U.S. Army Engineer Research and Development Center, Vicksburg, MS.

Zlotnik, V.A., and Zurbuchen, B.R. **1998**. Dipole probe: Design and field applications of a single- borehole device for measurements of vertical variations of hydraulic conductivity. *Ground Water* vol. 36, no.6: 884-893.

Appendix A: Well Skin Velocity Determination

The formation-well casing interface is an area of interest in many pumping wells. This area, known as the well skin, can have a great effect on the results of aquifer tests. These effects are only sparsely reported in the groundwater literature. The available studies show that skins are likely caused by compaction of the formation during well construction, invasion of drilling mud and fines into the aquifer, or clogging of the well screen itself (Barrash *et al.*, 2006, Novakowski, 1989). Much of the available research has been theoretical and resulted in models that show well-skin effects may lead to inaccurate aquifer characterization (Barrash *et al.*, 2006, Ramey and Agarwal, 1972). Some have suggested that hydraulic conductivity has been inaccurately estimated by 1-2 orders of magnitude in single-well aquifer tests due to the presence of well skins (Hyder and Butler, 1995, Faust and Mercer, 1985, Moench and Hsieh, 1985). The skin effect finds relevance in this study because of preliminary results of the Dipole Flow and Reactive Tracer Tests suggest an early breakthrough of tracer that may be related to the well skin.

In order to investigate this phenomenon, wells were constructed with PVP style detectors on the outside of the casing (Chapter 3). These wells, one with filter pack and one without, were used to monitor the breakthrough of saline tracer along the well skin of an operating well. Two detectors were placed approximately 15 cm apart on the well casing and the arrival of tracer at each detector was used to determine the velocity.

Results

The velocity in the skin zone is very fast. In the case of the filter packed well, the average velocity is ~8500 cm/day (Table 1). These velocities were determined at a pumping rate of 300 mL/min, which is slower than used in most DFRTTs. Tests conducted at higher pumping rates had results that were hard to interpret because the peaks arrived too close together. This was also a problem for the tests conducted in the well without a filter pack. The resolution of the datalogger was not sufficient to discern the difference in arrival time precisely. However, the velocity appears to be greater than 100,000 cm/day. This results in a nearly instantaneous transmittal of tracer from the injection screen to the extraction screen. This instantaneous response is useful because it allows for the start time of DFRTT results to be more precisely determined for the purpose of modeling and aquifer characterization.

Table 1: Well skin velocity data from well MWB. This well has no filter pack and the detectors are 15.8 cm apart. The velocity data here is difficult to interpret because the datalogger resolution was not high enough.

Month	Test	Peak	Detector	Time 1	Time 2	Average	Velocity
June	4	1	1	0.0919	0.1031	0.0975	
June	4	1	2	0.1008	0.1056	0.1032	66526
June	4	2	1	0.1838	0.1961	0.1900	
June	4	2	2	0.1883	0.1972	0.1928	135429
June	5	1	1	0.5489	0.5533	0.5511	
June	5	1	2	0.5531	0.5625	0.5578	56597
June	5	2	1	0.6422	0.6456	0.6439	
June	5	2	2	0.6425	0.6469	0.6447	474000
Sept	2	1	1	0.0839	0.0861	0.0850	
Sept	2	1	2	0.0839	0.0853	0.0846	-910080
Sept	2	2	1	0.1372	0.1450	0.1411	
Sept	2	2	2	0.1403	0.1478	0.1440	130011
Sept	3	1	1	0.6564	0.6597	0.6580	
Sept	3	1	2	0.6561	0.6606	0.6583	1312615
Sept	3	2	1	0.7561	0.7597	0.7579	
Sept	3	2	2	0.7594	0.7608	0.7601	169791
Sept	4	1	1	1.1250	1.1283	1.1267	
Sept	4	1	2	1.1244	1.1292	1.1268	2437713
Sept	4	2	1	1.2222	1.2244	1.2233	
Sept	4	2		1.2236	1.2278	1.2257	159105

Table 2: Well skin velocity data from well MWA. This well is completed with a filter pack and the detectors are 14.7 cm apart. The average velocity is 8510 cm/day.

Month	Test	Peak	Detector	Time 1	Time 2	Average	Velocity
June	1	1	1	0.0719	0.07472	0.0733	
June	1	1	2	0.1161	0.1208	0.1185	7815.88
June	1	2	1	0.2325	0.2358	0.2342	
June	1	2	2	0.2842	0.2861	0.2851	6921.42
June	1	3	1	0.4089	0.4286	0.4188	
June	1	3	2	0.4647	0.4692	0.4669	7320.35
June	2	1	1	0.7672	0.7725	0.7699	
June	2	1	2	0.8033	0.8058	0.8046	10160.64
June	2	2	1	0.9144	0.9386	0.9265	
June	2	2	2	0.9569	0.9783	0.9676	8581.62
June	2	3	1	1.095	1.1031	1.0990	
June	2	3	2	1.1258	1.1497	1.1378	9104.52
June	3	1	1	1.4392	1.4419	1.4406	
June	3	1	2	1.4839	1.4894	1.4867	7651.08
June	3	2	1	1.5975	1.6036	1.6006	
June	3	2	2	1.6469	1.6497	1.6483	7384.19
June	3	3	1	1.7681	1.7969	1.7825	
June	3	3	2	1.8094	1.8344	1.8219	8944.23
Sept	1	1	1	0.0442	0.0456	0.0449	
Sept	1	1	2	0.0850	0.0875	0.0862	8524.03
Sept	1	2	1	0.1803	0.1897	0.1850	
Sept	1	2	2	0.2150	0.2303	0.2226	9373.28
Sept	1	3	1	0.3322	0.3333	0.3328	
Sept	1	3	2	0.3750	0.3786	0.3768	8013.12
Sept	2	1	1	0.6606	0.6614	0.6610	
Sept	2	1	2	0.6981	0.7031	0.7006	8912.84
Sept	2	2	1	0.7872	0.8086	0.7979	
Sept	2	2	2	0.8278	0.8472	0.8375	8912.84
Sept	2	3	1	0.9222	0.9656	0.9439	
Sept	2	3	2	0.9761	0.9819	0.9790	10040.16

Appendix B: Visual MODFLOW Model

In order to evaluate field velocity data, a model was created to simulate the effect of heterogeneity on the velocity and breakthrough curves. The model consists of a 10 x 10 x 10 m (x, y, z; width/length/depth) domain with the dipole device centrally located. The dipole was represented by two pumping wells, one extraction well and one injection well placed at different depths. The cells between the wells were inactive and represented the portion of the well bore closed by a packer. The domain was highly discretized in the region near the pumping well. The water table was represented 0.5m below ground surface (bgs) by constant-head boundaries. A small gradient (0.007) was imposed in some cases using slightly different constant-head boundaries. The tracer was modeled using the MT3DMS engine with a conservative tracer at a pumping rate of 700 mL/min. The system was generally modeled for 4 hours, but some longer runs were used to evaluate different hydraulic conductivity regions. When velocities were compared, the pumping rate was 1100 mL/min. Other general model input data can be found in Table B.1. A list of different cases presented in Chapter 4 can be seen in table B.2.

Table B.1: Visual MODFLOW model parameters.

Parameter	Value	Source
Specific Storage	1.00E-05	MODFLOW Default
Specific Yield	0.3	Nwankwor 1984
Porosity	0.4	Brewster *et al.* 1995
Longitudinal Dispersivity	0.01	Sudicky *et al*. 1993
Injection well screen dimensions	5.24m to 5.4 m	Dipole prototype dimensions measured from bottom up
Extraction well screen dimensions	4.8m to 4.96 m	Dipole prototype dimensions measured from bottom up
Tracer injection time	10 min	Field Conditions

Table B.2: Visual MODFLOW input parameters used to simulate breakthrough curve behavior at a flow rate of 700 mL/min.

Trial	Breakthrough Curve Results	Overall Hydraulic Conductivity (m/s)	Secondary Hydraulic Conductivity (m/s)	Model Domain Figure
Homogeneous	Figure 4.8 Homogeneous	5.80E-05	N/A	Figure B.1
Homogeneous with Gradient	Identical to Homogeneous	5.80E-05	N/A	Figure B.1
Shallow Lower K zone	Figure 4.8 A	5.80E-05	3.87E-05	Figure B.2
Central High K zone	Figure 4.8 B	3.87E-05	5.80E-05	Figure B.3
Deep Lower K zone	Figure 4.8 C	5.80E-05	3.87E-05	Figure B.4
High Conductivity zone near well	Figure 4.8 D	3.87E-5	5.80E-5	Figure B.5
High Conductivity zone proximal to well	Figure 4.10 A	5.80E-05	8.70E-05	Figure B.6
Low conductivity zone proximal to well	Figure 4.10 B	5.80E-05	1.93E-05	Figure B.6
High Conductivity zone proximal to well 2	Figure 4.11 B	5.80E-05	6.50E-05	Figure B.6

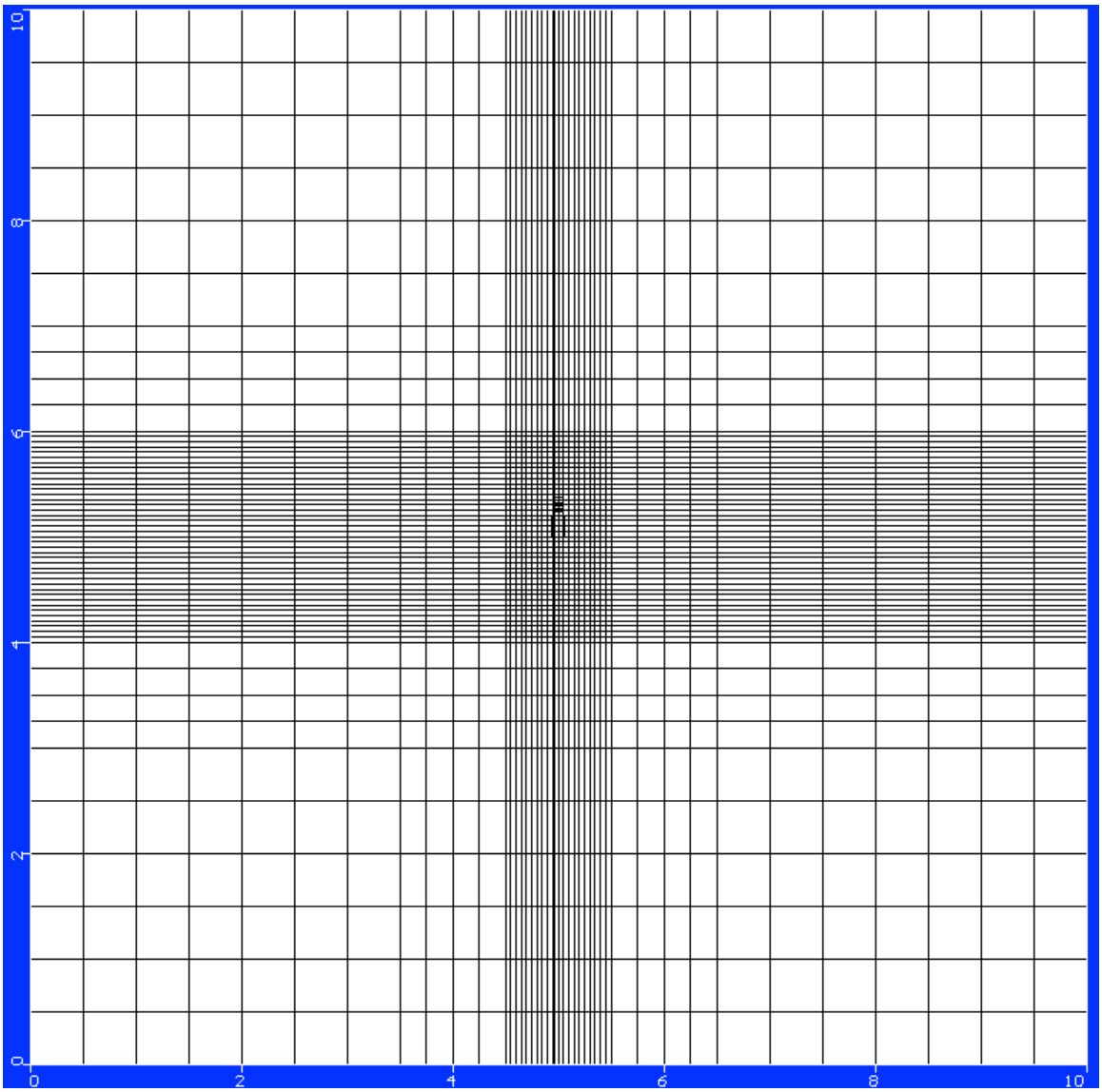

Figure B.1: A cross section of the hydraulic conductivity domain used for the homogeneous and homogeneous with gradient modeling cases. The dimensions are 10m by 10m.

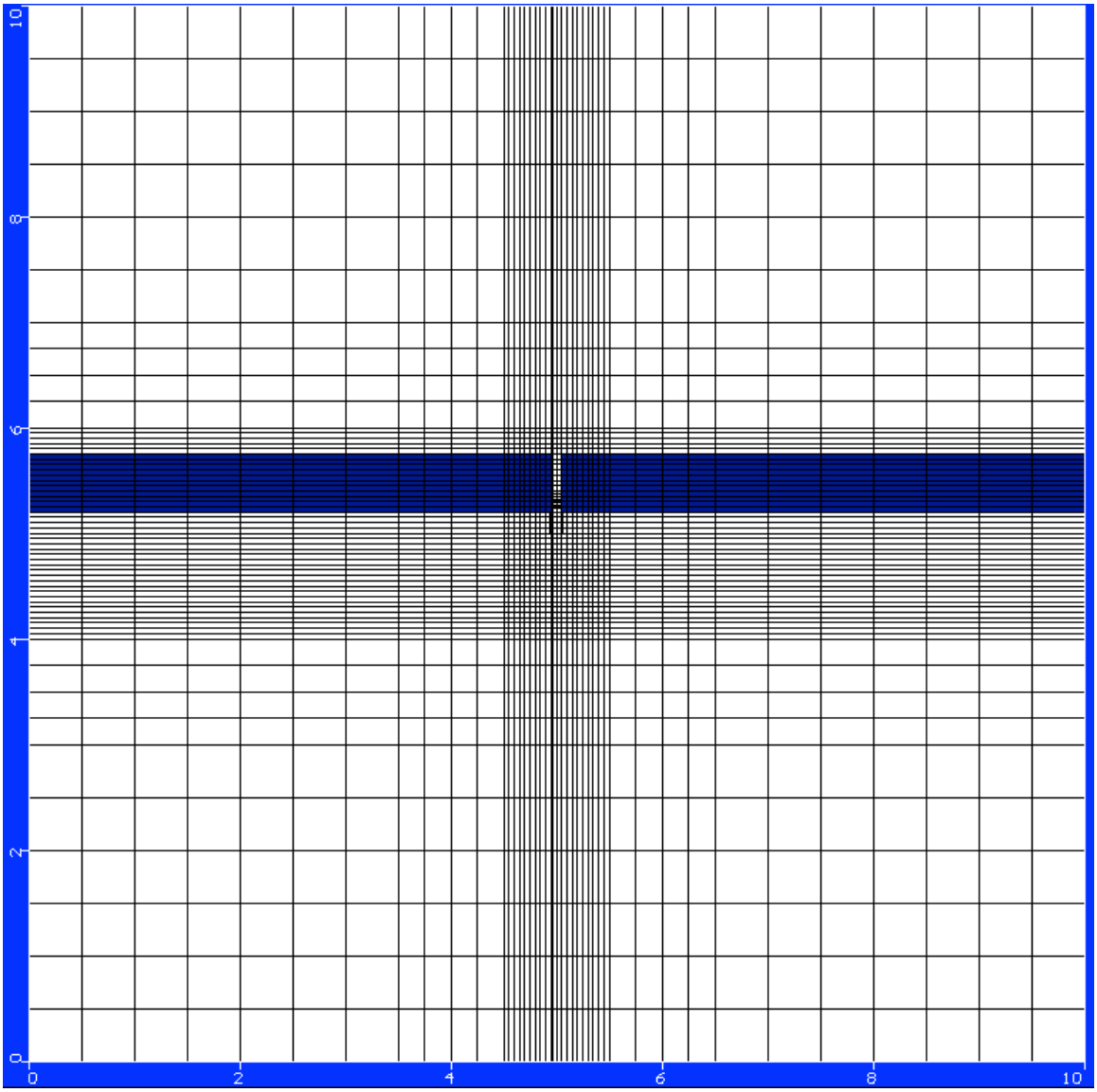

Figure B.2: A cross section of the hydraulic conductivity domain used to simulate a low hydraulic conductivity zone near the injection portion of the dipole well. The white zone has a hydraulic conductivity of 5.8 x 10^{-5} m/s and the blue zone has a hydraulic conductivity of 3.87 x 10^{-5} m/s. The dimensions are 10m by 10m.

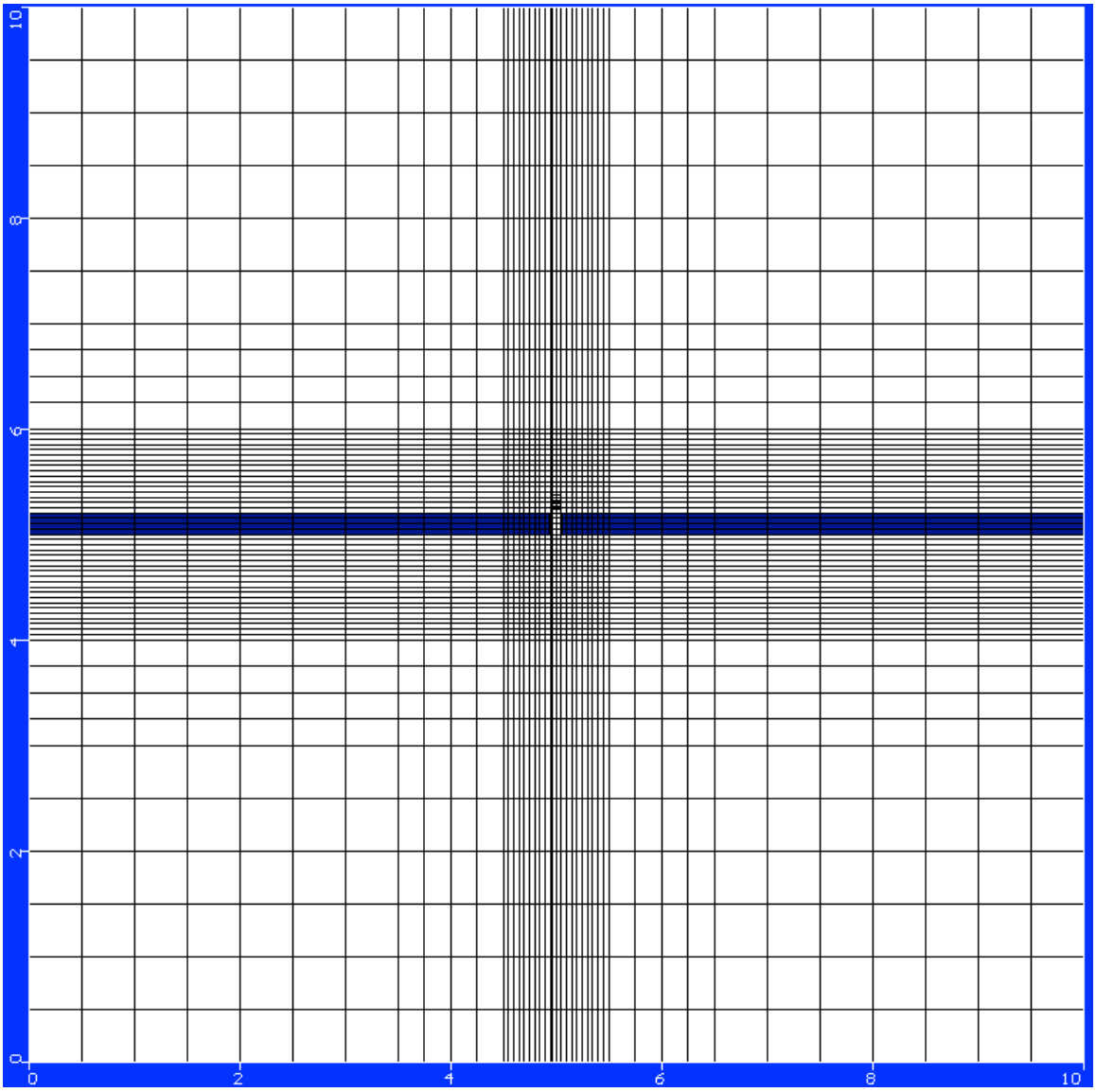

Figure B.3: A cross section of the hydraulic conductivity domain used to simulate a high hydraulic conductivity zone between the screen of the dipole well. The white zone has a hydraulic conductivity of 3.87 x 10^{-5} m/s and the blue zone has a hydraulic conductivity of 5.8 x 10^{-5} m/s. The dimensions are 10m by 10m.

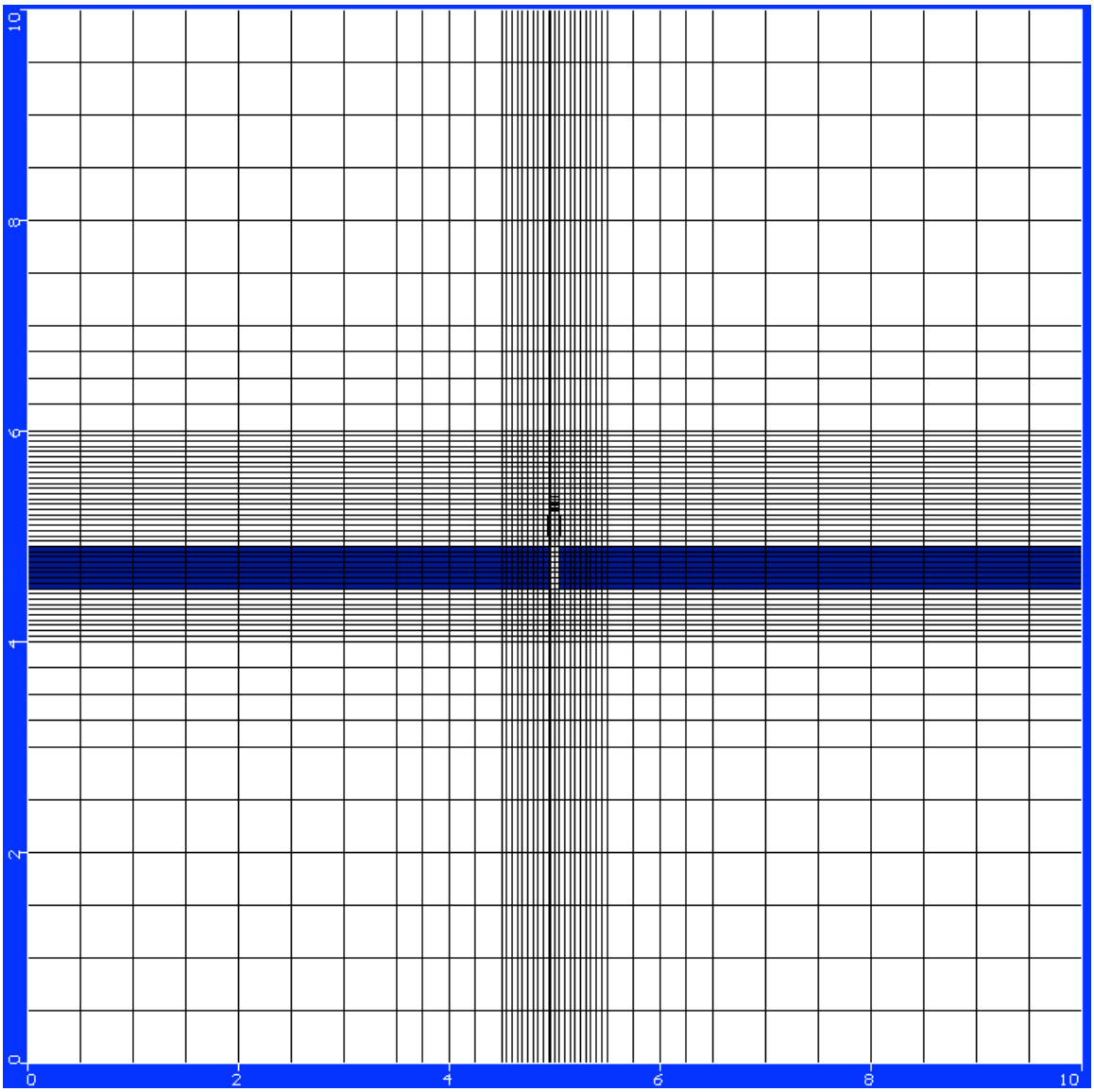

Figure B.4: A cross section of the hydraulic conductivity domain used to simulate a low hydraulic conductivity zone near the extraction screen of the dipole well. The white zone has a hydraulic conductivity of 5.8 x 10^{-5} m/s and the blue zone has a hydraulic conductivity of 3.87 x 10^{-5} m/s. The dimensions are 10m by 10m.

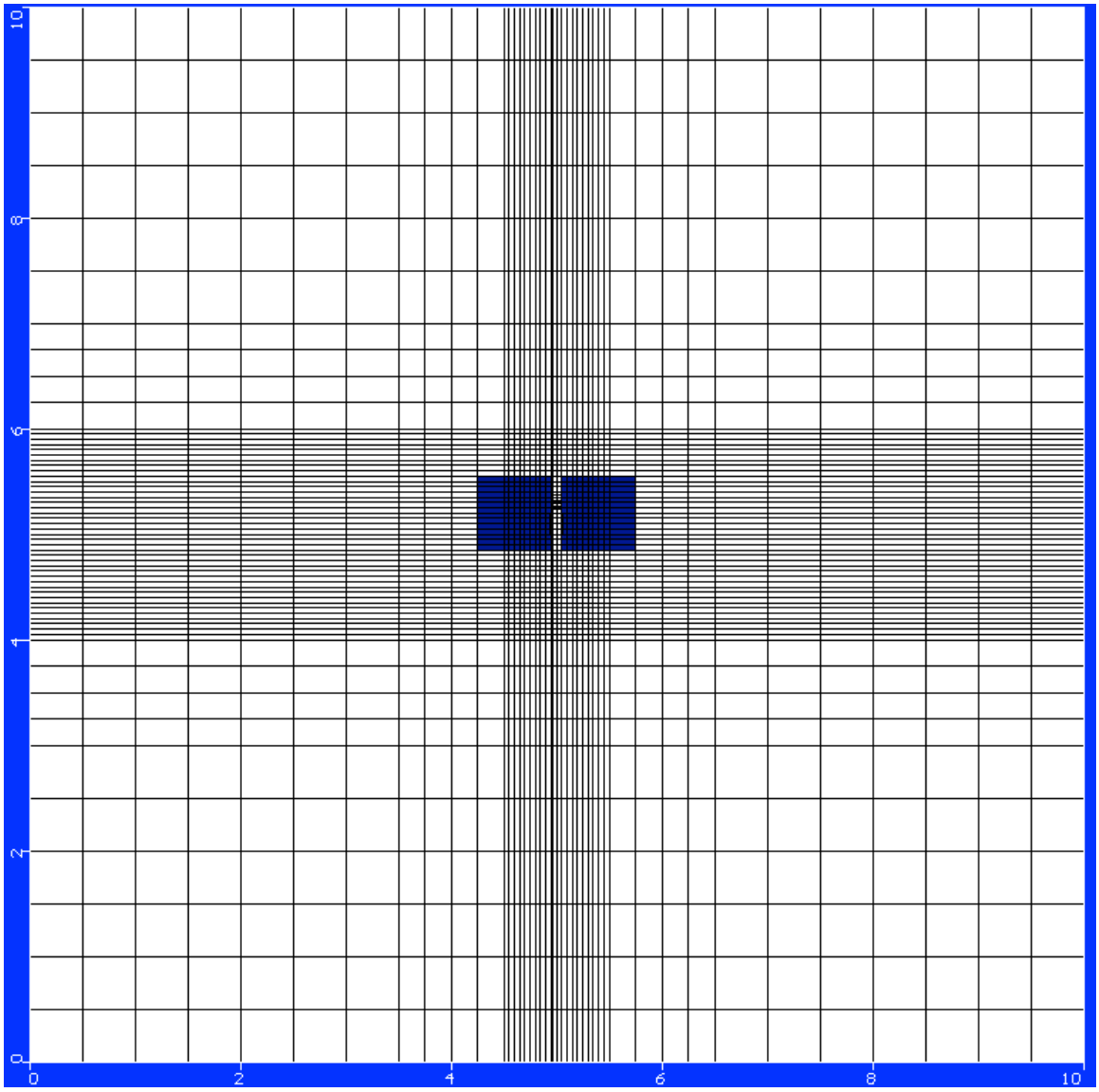

Figure B.5: A cross section of the hydraulic conductivity domain used to simulate a discontinuous high hydraulic conductivity zone near the dipole well. The white zone has a hydraulic conductivity of 3.87 x 10^{-5} m/s and the blue zone has a hydraulic conductivity of 5.80 x 10^{-5} m/s. The dimensions are 10m by 10m.

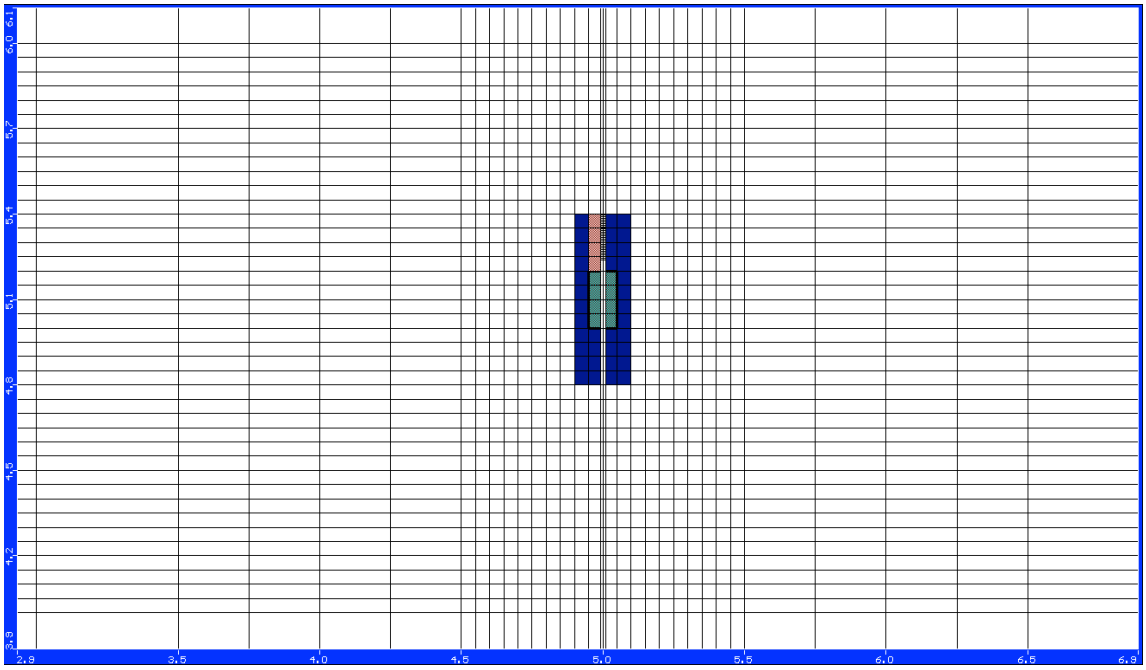

Figure B.6: A cross section of the hydraulic conductivity domain used to simulate a high hydraulic conductivity zone proximal to the screen of the dipole well. The white zone has a hydraulic conductivity of 5.8 x 10^{-5} m/s and the blue zone has the hydraulic conductivities reported in Table B.2. The scale here is smaller than the other figures (B.1-B.5) to capture the detail near the well. The dimensions show the region from 2.9 to 6.8 m (in x) and 3.9 to 6.1 m (in z).

Appendix C: Field Velocity Data

Table C.1: Velocity data obtained June 2009.

Probe	Test	Vel (xy)	Vel (z)	Vtot
20-11	1	0	33	33
20-11	3	10.8	21	23.61440238
20-F	1	20	10.5	22.588714
20-7	1	0	-192	192
20-7	4	0	-200	200
20-C	1	43	0	53
20-C	3	25	0	12
20-C	4	27	0	16
20-8	1	0	173	173
20-8	3	0	46	46
20-8	4	0	63	63
25-2		19	0	19

Table C.2: Velocity data obtained September 2009

Probe	Test	Horizontal Velocity (cm/day)	Vertical Velocity (cm/day)	Total Velocity (cm/day)
20-2	1	6.3	4.7	7.860025445
20-2	2	3.6	5.1	6.242595614
20-2	4	3.5	5.5	6.519202405
20-11	1	6.9	0	6.9
20-11	2	6.2	0	6.2
20-11	3	8.1	0	8.1
20-11	4	9.7	0	9.7
20-F	1	105	228	251.0159357
20-F	2	107	273	293.2200539
20-F	3	97	0	97
20-C	None			
20-A	1	29	43	51.86520992
20-A	2	29	47	55.22680509
20-A	3	37.7	0	37.7
20-A	4	52.5	0	52.5
20-6	2	0	-18.9	18.9
20-6	4	0	-19	19
20-22	1	0	-6.25	6.25
20-22	3	0	-5.6	5.6
20-22	4	0	-5.9	5.9
20-7	1	0	-242	242
20-7	2	281	-364	459.8445389
20-7	3	0	-307.7	307.7
20-7	4	0	-306.5	306.5
20-8	1	0	-281.7	281.7
20-8	2	0	-278	278
20-8	3	0	-230	230
20-8	4	0	-203	203
20-20	1	0	-5.8	5.8
20-20	4	0	-4.3	4.3
20-15	none			
25-6	2	30.4	0	30.4
25-6	3	28.4	-13.7	31.53173005
25-6	4	28.5	-13.4	31.4930151
25-E	1	12.4	-38.6	40.54281687
25-E	2	12.4	-56.7	58.04007236
25-D	None			
25-2	3	48.9	-34.7	59.96082054
25-B	2	4.3	0	4.3
25-G	None			

Appendix D: The effect of PVP diameter on measured velocity.

The point velocity probe presented here was tested in the laboratory as part of development. During this testing, the velocity estimates from the probe were compared to those from a larger, previous PVP design. The PVPs were tested simultaneously and therefore the actual velocity measured by each probe is nearly the same. However, there are some differences between the data sets collected with each probe. These results suggest there is a possible size dependence on the velocity estimate (Figure D.1). The smaller PVP (presented here) consistently returns lower velocity estimates than those of the larger PVP. The bias is nearly 20%. However, it should be noted that the average measurement error of the PVP is 15% and the uncertainty in the calculated velocity is 23%. Nevertheless, these preliminary findings suggest that the effect of PVP size on velocity estimates needs to be further explored. There is no mathematical or theoretical dependence on diameter, which further complicates the explanation of the results. It is possible the smaller PVPs are sensitive to small-scale heterogeneities that do not affect the larger PVP. However, these differences are expected to be minimal in a laboratory sand tank filled with commercially available sand.

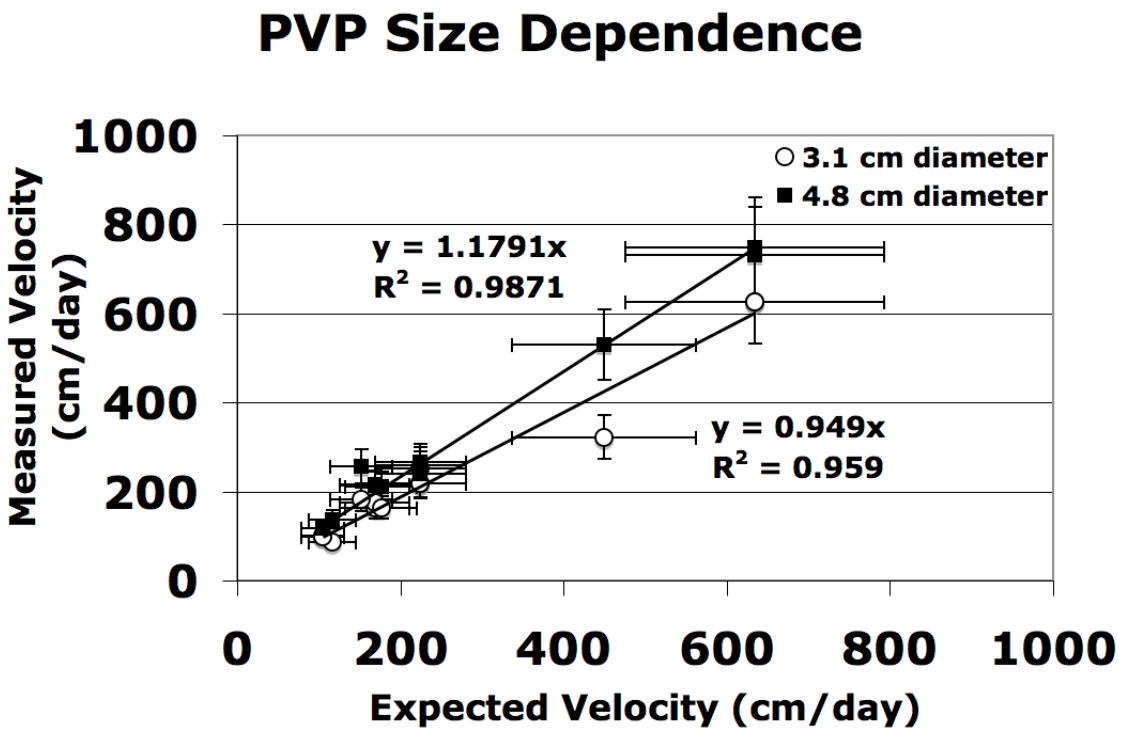

Figure D.1: The measured and expected velocities of two different-sized PVPs show a possible measurement dependence on PVP size. The error bars represent the average measurement error for the PVPs (15%) and the 23% error associated with the uncertainty in determining the cross-sectional area and porosity for the expected velocity.